THE ASTROPHYSICAL JOURNAL, 326:967–987, 1988 March 15

THE MAGNETIC FIELD AND ABUNDANCE DISTRIBUTION GEOMETRY OF THE PECULIAR A STAR 53 CAMELOPARDALIS

J. D. LANDSTREET[1]
Department of Astronomy, University of Western Ontario, and Institut für Theoretische Astrophysik der Universität Heidelberg
Received 1987 June 9; accepted 1987 September 14

ABSTRACT

New spectra have been obtained of the magnetic Ap star 53 Cam, well spaced through its 8.03 day rotation period, covering the spectral regions λλ3900–3960 and 4250–4315. These data, and previously obtained Hβ Zeeman analyzer observations of the longitudinal field strength, have been used to derive models of the magnetic field geometry and the abundance distributions of Ca, Cr, Fe, Sr, and Ti. The models have been obtained by use of a new line synthesis program that incorporates the effects of an assumed magnetic field and abundance distribution into the calculation of line profiles. Calculated profiles are compared with observations, and the model assumed is altered until good agreement between calculation and observation is obtained.

The magnetic field of 53 Cam may be modeled using colinear dipole, quadrupole, and octupole components of polar strength (at the strong negative pole) of −16,300, −7300, and +4900 G, respectively. Both the inclination of the rotation axis and the obliquity of the field axis to the rotation axis are large, with values of 64° and 82°. The abundance distributions of the elements modeled appear to be axisymmetric about the magnetic axis. Cr and Fe appear to be roughly uniform in distribution with mild depletions (times ~2) around the magnetic equator relative to the poles. Sr is similarly distributed, but with somewhat greater abundance contrast. Ca and Ti seems to be much more nonuniform in distribution. Each has one region of high abundance (Ti around the strong negative magnetic pole, Ca around the weak positive pole) and considerably smaller average abundance elsewhere on the star.

From an accurately determined value of $v \sin i = 13$ km s^{-1} and the constraint on the inclination i provided by the magnetic model, it is possible to derive a radius of $R/R_\odot = 2.3 \pm 0.4$, a luminosity of $\log L/L_\odot = 1.4 \pm 0.17$, and a mass of $M/M_\odot = 2.0 \pm 0.3$ for 53 Cam.

Subject headings: line profiles — stars: individual (53 Cam) — stars: magnetic — stars: peculiar A

I. INTRODUCTION

a) *The Astrophysical Problem*

It has been known for many years that some upper main-sequence A and B stars whose spectra are characterized by anamalous line strengths of such chemical elements as He, Si, Cr, Fe, and Eu possess rather strong magnetic fields of roughly dipole structure (Babcock 1958). Such stars also frequently exhibit variability in the strengths of the spectral lines of some (but not all) elements. These magnetic spectrum variables usually show changes in the line-of-sight or longitudinal component of the magnetic field (the component that is normally measured), and when both spectral lines and the magnetic field vary, they do so periodically, with the same period for both spectrum and magnetic variations. Furthermore, when the period of variation is short (a few days or less), such variables usually have projected rotation velocities of 10–100 km s^{-1}, with large $v \sin i$ and short period strongly correlated, while long-period variables (which can have periods up to some years) have in general extremely sharp lines.

These facts have led to the widespread acceptance of the oblique rotator model for these stars (e.g., Deutsch 1958*a*; Preston 1967, 1971*a*; Wolff 1976, 1983, pp. 34–36, 66–68; Borra, Landstreet, and Mestel 1982; Khokhlova 1985). In this model the star is assumed to be permeated by a magnetic field of roughly dipolar structure with its axis of symmetry inclined to the rotation axis of the star by an angle β. The star is assumed to rotate with the observed period, and the observed changes in the longitudinal component of the magnetic field are caused by the changing aspect of the field as it rotates. Similarly, the spectrum variations are assumed to be due to nonuniform distribution of some elements laterally in the photosphere. Since the nonuniform distribution of material is presumably caused by the field, the abundance distributions will not be symmetric about the rotation axis if β is nonzero. The spectrum variations are then produced, like the magnetic variations, by changing aspect.

It is remarkable that when qualitative oblique rotator models of individual stars are constructed from examination of the observations, one frequently finds that the abundance inhomogeneities are dominated by large patches where one or several elements are overabundant. These patches usually seem to be located near one of the magnetic poles, but elements that are found to be overabundant near one pole are not necessarily the same as those overabundant near the other pole. Thus, for example, one might find that some iron-peak elements are overabundant near one magnetic pole, while the rare earths are overabundant near the other pole.

Some years ago, detailed models of the magnetic field structure and surface composition distributions were constructed from photographic measurement of effective magnetic field variations and line strength variations for the stars HD 125248 = CS Vir (Deutsch 1958*a*) and HD 112413 = α^2 CVn

[1] Visiting Astronomer, Canada-France-Hawaii Telescope, operated by the National Research Council of Canada, the Centre National de la Recherche Scientifique of France, and the University of Hawaii.

(Pyper 1969). Important limitations to the accuracy of these models arise from the low signal-to-noise ratio of the data used, and from inadequate modeling of the magnetic data (Borra 1974). More recently, much modeling has been done with data of higher signal-to-noise ratio. Modeling efforts have also been improved by the use of data not utilized in earlier work: line profiles rather than simply equivalent widths and radial velocities, and surface magnetic field measurements (for a few stars of low $v \sin i$ and large field strength) in addition to the normal longitudinal field observations. However, investigators have generally modeled either the magnetic field geometry (e.g., Preston 1969*a*, 1970; Wolff and Wolff 1970; Borra and Landstreet 1977, 1978) or the abundance distribution geometry (e.g., Khokhlova 1970; Rice 1970; Mihalas 1973; Megessier 1975; Megessier, Khokhlova, and Ryabchikova 1979; Wehlau *et al.* 1982; Goncharskii *et al.* 1983; Van Rensbergen, Hensberge, and Adelman 1984), but not both at once. At present, there is not a single star for which really good maps of both the magnetic field geometry and the abundance distributions of even a few chemical elements are available.

An important reason for studying magnetic field geometry and abundance distributions together is that one cannot readily determine either the magnetic geometry or the abundance distributions without knowing something about the other. Many of the spectral lines used for abundance determinations split into rather complex Zeeman patterns, and if the local field is a few kilogauss or more, this splitting may significantly desaturate a line and increase its equivalent width substantially over the value that would occur in the absence of a field. Important errors in inferred abundance can result. Furthermore, local variations in magnetic field strength can lead to variations in local line strength, and hence to spectrum variability, even in lines of elements uniformly distributed over the star. Conversely, if the magnetic field is measured using spectral lines of elements that are not distributed uniformly over the stellar surface, then the field is not sampled uniformly over the stellar disk. Errors in the inferred field geometry can occur if this effect is ignored. Thus, to obtain either an accurate field geometry or an accurate abundance distribution, both should actually be found.

Such complete models are also important for comparison with theoretical predictions of expected field geometries and abundance distributions. It is widely believed that the abundance anomalies found in the atmospheres of the peculiar stars are the result of competition between gravitational settling of trace atoms in the predominantly hydrogen photosphere, and radiation pressure levitating those atoms that are not too abundant and that have numerous lines (or strong continua) in spectral regions where much radiation flux emerges from the star (Michaud 1970). Competition between these two processes can apparently produce anomalies both in nonmagnetic and in magnetic stars, but in magnetic stars the field appears to affect the diffusion process, so that the abundance of a particular element can be different in different parts of the magnetic field at a given time, and spectral patches are observed. This may occur either as a result of Zeeman splitting which desaturates lines and alters the vertical radiation force on the atoms, or as a result of horizontal migration high in the photosphere, guided by the magnetic field lines. Theoretical calculations predicting the types of abundance distributions that might be expected for a few elements due to horizontal migration are beginning to appear (Vauclair, Hardorp, and Peterson 1979; Alecian and Vauclair 1981; Michaud, Megessier, and Charland 1981, hereafter MMC; Megessier 1984). Using observations to test these calculations clearly requires information about the structure of abundance anomalies with respect to the magnetic field geometry, and thus requires precisely the kind of accurate composite field and abundance maps that are not now available.

For these reasons I began a few years ago to acquire high-resolution, high signal-to-noise spectra of a number of magnetic Ap and Bp stars, well spaced throughout the period of magnetic variation, and to complete the measurement of longitudinal magnetic field curves of these stars using the Balmer line Zeeman analyzer if they were not already satisfactory. Because magnetic observations of the longitudinal field alone (which in the usual case of essentially sinusoidal magnetic variation furnishes two constraints on the magnetic model) are not sufficient to specify the magnetic geometry of even a simple centered dipole completely, and because one of the main goals of this project is to obtain well-constrained magnetic field models, virtually all the stars observed have sufficiently strong magnetic fields (several kilograms or more) that the line profiles are noticeably affected by magnetic splitting and intensification, so that the mean surface field of the star can be measured through the rotation cycle and provide enough extra information to constrain the magnetic field model fairly closely. Furthermore, most of the stars observed are known to have at least some variable elements, so that interesting abundance distribution mapping can be done. A final observational constraint has been that all of the stars in the primary program have periods short enough (less than ~ 20 days) for at least a large part of one cycle to be observed in one long coudé observing run. Fairly complete sets of observations for this program have now been obtained for the stars HD 24712 = HR 1217, HD 32633, HD 65339 = 53 Cam, HD 125248 = CS Vir, and HD 215441 = Babcock's star. Less complete observations are available for several other stars. This paper will be limited to a discussion of some of the data available for HD 65339 = 53 Cam and of the techniques used to model it; other stars will be discussed in future papers.

b) Modeling Approaches

Three different approaches have been used to infer the abundance distributions of various elements over the surface of a star from observations of equivalent width and radial velocity or from profile measurements. These are reviewed and critically analyzed by Khokhlova (1985). The first of the methods, developed by Deutsch (1958*b*) and used with some modification by Pyper (1969), Rice (1970), and Megessier (1975), consists in expanding the local equivalent width distribution over the stellar surface in spherical harmonics up to the second order. The observed equivalent width and radial velocity variations are then expanded in Fourier series, and the expansion coefficients for the abundance distribution are determined from the Fourier coefficients. A similar method is used to determine the magnetic field distribution from photographic measurements of the longitudinal (or effective) magnetic field strength as a function of phase. This technique has the advantage that it is fairly straightforward mathematically and does not involve guessing at the needed distributions. However, it makes little use of the information contained in the observed line profile, since comparison is made only with the equivalent width and radial velocity of the line. Detailed structure in the observed profiles, which may contain much information about the abundance distribution and magnetic field structure, is

ignored. In addition, the small number of spherical harmonics used and the simple local profiles assumed may produce a poor representation of the actual abundance distribution of an element. A final drawback is that the resulting element distributions are maps of equivalent width rather than of abundance.

A second method is to start with an assumed model of the abundance distribution (or field geometry), to calculate as accurately as desired the resulting flux (and perhaps polarization) profiles of suitable lines, and to compare the result with observations. The model is modified and the calculation is repeated as often as necessary to achieve agreement between the calculated and observed profiles. This technique has been used by Khokhlova (1970), Khokhlova and Ryabchikova (1975), and Megessier, Khokhlova, and Ryabchikova (1979). The method has the great advantages over the expansion technique that comparison is made with observed line profiles rather than only with their low-order moments, so that rather finer scale spatial structures on the stellar photosphere can be identified and modeled than with the expansion technique. However, it is not easy to force convergence of the assumed model to one that accurately represents the observations in a small number of iterations, so that the technique is computationally very expensive.

Most recently, several Soviet astronomers have explored the possibility of using modern numerical techniques to invert the integral equation that relates the observed line profile to the local intrinsic intensity profile and the (unknown) abundance distribution (Goncharskii *et al.* 1977, 1982, 1983; Wehlau *et al.* 1982; Khokhlova, Rice, and Wehlau 1986). This technique may also be usable for obtaining models of magnetic geometry (Piskunov 1986). Like the expansion technique, this is a mathematically fairly straightforward method that involves a minimum of guess work, but like direct modeling it is capable of resolving fairly fine structure on the stellar photosphere. On the other hand, in practice the local intensity profile must be represented by a fairly simple analytical formula, and the maps so far obtained show the variation of equivalent width over the photosphere rather than real abundance variations.

The stars of interest for this program in general have rather large magnetic fields, which of course is essential if the spectral line profiles are to provide useful constraint on the field geometries. However, this fact also means that the local intensity profiles will vary quite considerably from one place to another on the stellar surface, both as a function of local abundance and as a function of local magnetic field strength and orientation. Piskunov (1986) has discussed how such lines could be modeled by numerical inversion of the associated integral equation, but his technique assumes that the local intensity profiles are described by a Milne-Eddington type of solution to the coupled equations of transfer for the Stokes parameters (Unno 1956). Although this solution is analytically convenient, it is not very accurate, and it is not certain that the resulting model will provide a very accurate description of the observed star. For this reason, it seems preferable to me to explore the utility of a direct modeling approach, in which accurate local model intensity profiles are calculated as solutions of the real (depth-dependent) equations of transfer, integration over the disk is performed, and the resulting calculated line profile is compared to the observed one. It is not clear *a priori* that this technique can be made to converge satisfactorily either to the observed line profiles or to a unique model, but this is one of the questions to be explored in this study. This approach has in any case the considerable advantage that physically interesting quantities such as real abundances are directly obtained from the solution, and if a satisfactory solution is found, there is not much lingering doubt about the possible effects on the solution of greatly simplified modeling of local profiles.

The star HD 65339 = 53 Cam = AX Cam is an obvious star to choose as a starting point for a modeling project of the sort just described. It has a large magnetic field, discovered by Babcock (1958). The effective field ranges from about +4 kG to −5 kG (Babcock 1960; Borra and Landstreet 1977). The field is sufficiently large that some of the spectral lines are visibly resolved into Zeeman components (Preston 1969*b*), and the mean surface field is rather easy to measure; it ranges between ∼10 kG at the positive effective field extremum to 17 kG at the negative field extremum (Huchra 1972). The star is also a strong spectrum variable; Babcock (1958) notes that Mg and Ti are variable, and a more detailed study of spectrum variations by Faraggiana (1973) revealed substantial variations in Ca, Ti, Sr, and Eu, as well as small variations in the strengths of lines of a number of other elements. Finally, the star has a well-determined period so that various observations can be phased together (Borra and Landstreet 1977), and this period, ∼8.03 days, is a convenient length for obtaining a series of spectrograms well-distributed in phase during a single coudé observing run.

The star is also a convenient starting point for modeling experiments because it has previously been modeled on several occasions. The geometry of the magnetic field has been discussed by Landstreet (1970), Huchra (1972), and Borra and Landstreet (1977). A model for the possible distribution of several atomic species over the surface, based on possible effects of horizontal diffusion (due to inclined lines of force in the upper layers of the atmosphere) has been proposed by MMC on the basis of Faraggiana's (1973) observations.

The present paper will be concerned primarily with modeling the abundance distribution geometries of a few iron peak elements and the magnetic field geometry of 53 Cam. In the next section, I shall describe the new spectroscopic material obtained for this program. In § III, the spectral line synthesis program used to generate line profiles for model stars with specified magnetic geometries and abundance distributions will be described. The derivation of a model for 53 Cam will be the subject of § IV, and two final sections will discuss and summarize the results.

II. OBSERVATIONS

a) Spectroscopy

Spectra for this project were obtained with the coudé spectrograph of the Canada-France-Hawaii 3.6 m telescope on eight successive nights in 1984 February. The f/7.4 camera and 830 lines mm^{-1} grating were used with the 1872 diode Reticon detector (Campbell *et al.* 1981), giving a spectrum ∼65 Å long at 0.1 Å resolution. Only two 65 Å windows in the spectrum of 53 Cam could be observed to the desired signal-to-noise ratio each night. I decided to observe the region λλ3900–3965 as one of the two windows, because of the presence of the strong and highly variable K line of Ca II, along with many lines of Fe I and Fe II. For the second window, I looked for a wavelength interval containing several lines of each of the abundant iron peak elements Ti, Cr, and Fe; an additional constraint was the requirement that a reasonable variety of magnetic sensitivities (*z*-values) be present to enable the broadening effects of the

TABLE 1

JOURNAL OF SPECTRAL OBSERVATIONS OF 53 CAMELOPARDALIS

Julian Date (2,445,700+)	Duration (min)	Wavelength Range (Å)	Phase
45.900.....	75	3891–3957	0.169
46.007.....	100	4250–4316	0.182
46.906.....	90	3899–3965	0.294
46.990.....	63	4250–4316	0.304
47.936.....	118	4250–4316	0.422
48.898.....	90	3897–3964	0.542
48.982.....	67	4250–4316	0.553
49.907.....	91	3897–3964	0.668
49.989.....	86	4250–4316	0.678
50.888.....	68	3897–3964	0.790
50.955.....	44	4250–4316	0.798
51.893.....	75	3897–3964	0.915
51.975.....	70	4250–4316	0.925
52.893.....	75	3897–3964	0.040
52.981.....	116	4250–4316	0.051
53.909.....	82	4460–4526	0.166

magnetic field to be separated from those of rotation. The spectral window λλ4250–4315 fulfils all these requirements and is almost the only region between 3900 and 4600 Å that does. This region has reasonably strong lines of Ti II, Cr I and II, and Fe I and II, as well as the strong Sr II line at 4305 Å. Both Cr and Fe lines have a large range of z-values. Unfortunately, however, this window contains very few strong lines of rare earth elements, which contribute significantly to line blending, and serious modeling of rare earth abundances is very difficult with this spectral material. Only lines from the spectral region λλ4250–4315 will be modeled in a detailed way for the analysis of this paper.

Phases were calculated for all observations using the period given by Borra and Landstreet (1977),

$$\text{JD(positive crossover)} = 2{,}435{,}855.652 + 8.0267E\ . \quad (1)$$

This period is based on all published effective field measurements available over a time base of ~19 yr, and the accuracy is estimated to be approximately ±0.0002 days, which leads to an uncertainty in the phases of the present observations of only ~0.03 cycles relative to the zero point of the ephemeris, or an uncertainty in relative phase between the Balmer line Zeeman analyzer magnetic measurements of Borra and Landstreet (1977) and the present measurements of only ~0.01 cycle. This is a negligible phase uncertainty.

A journal of observations is given in Table 1, which lists the Julian Date at the midpoint of the observation, the duration in minutes of the full observation, the wavelength region observed, and the phase of the observation. It will be seen from this table that the phase coverage obtained is excellent.

b) *Reductions of Spectra*

The observations were reduced by M. Jewison using a reduction package developed for CFH Telescope Reticon spectra by P. K. Barker of the University of Western Ontario. The first step in the reductions is to determine the scale of pixel number versus wavelength. This is done using the iron hollow cathode lamp spectra observed at the beginning or end of the series of observations made with one grating setting. The required relation is obtained for the wavelength region by fitting a third-order polynomial to the measured pixel numbers of a number (usually nine) of well-exposed lines through the lamp spectrum. The resulting polynomial fit produces a relationship which predicts wavelengths for the hollow cathode lines that deviate from the assumed ones by typically 0.008 Å at 3930 Å and by 0.005 Å at 4280 Å. The polynomial fit is then used to calculate the wavelength for each pixel in the observed spectrum. This wavelength scale is reduced to the heliocentric frame of reference at a later stage in the reductions.

By comparing the wavelength versus pixel number relationships found from hollow cathode spectra taken early in the night with those taken later, it is possible to establish the stability of the coudé spectrograph against wavelength drifts and scale changes during the night. It is found that over a period of 5 hr (the maximum time spent on one grating setting) the wavelength drift of the spectrograph is almost always less than 0.01 Å, and the change in scale is never more than 0.01 Å over the 65 Å field viewed by the Reticon.

The next step is to divide the stellar spectrum by a lamp spectrum to correct for small pixel-to-pixel variations in sensitivity and amplifier gain. The flat-field lamp is a 500 W quartz-iodide lamp that is mounted before the last folding mirror of the coudé mirror train. An adjustable pupil in the beam renders the pencil of rays from the lamp similar to the ray pencil from the star. Flat-field exposures were usually obtained at the end of the observations made with one grating setting.

The stellar spectra obtained up to this point in the reductions are found to have a fairly significant continuum slope, due to the fact that the flat-field lamp has a considerably cooler temperature than the observed stars. In addition to the continuum slope, the continua of relatively line-free stars show some residual curvature, deviating from a straight line by up to 5% (peak-to-peak). This curvature varies from one spectrum to another, although it normally has the same qualitative character for all spectra of a dip somewhere near the middle of the spectrum relative to the ends. It is not clear what the origin of this effect is. However, it may be largely removed by fitting a sixth-order polynomial to continuum points spread through the spectrum, and then dividing the observed spectrum by the polynomial. This, of course, also removes the slope of the continuum and normalizes the observed spectrum to a continuum of 1.00. The effect of division of the spectrum of a star with a clear continuum level by such a polynomial is to reduce the peak-to-peak amplitude of remaining waves to ~1%. For stars such as 53 Cam that have extensive regions in which line absorption keeps the intensity below the continuum, such a fitting procedure is less straightforward, and its results are less easy to assess. However, the resulting spectra appear to be improvements over the unflattened ones.

The reproducibility of the spectra obtained has been tested by observing several times during the run a number of normal and Ap HgMn stars that are presumably not variable. The stars observed include α Lyr (HD 172167, A0 V), α Dra (HD 123299, A0 III), HR 6559 (HD 159834, A7 IV), ι CrB (HD 143807, Ap HgMn), and ν Her (HD 144206, Ap HgMn). HR 6559 and the HgMn stars are particularly suitable for determining how reproducible the observed spectra are, as they have numerous sharp and deep lines. These test spectra were generally exposed to a signal-to-noise level similar to that obtained for 53 Cam (2-400). When spectra from different nights are compared, the main differences appear to arise from variations in the continuum fitting, which do not normally exceed ~1%; from intrinsic radial velocity variations (α Dra, ι CrB, and ν Her are known to be members of close binary

systems); and from small changes in the focus of the spectrograph from night to night, which have no effect on observations of most stars but lead to noticeable variations in central depth and sharpness of the lines of intrinsically very sharp-lined stars such as ι CrB. There are also a few cosmic-ray flaws in most spectra exposed for more than a few minutes; these appear as small emission spikes normally ~ 3 or 4 pixels wide. Overall, repeated spectra agree to within less than 1% when the continua are matched locally, and even without this the differences are rarely much more than 1%. This is an adequate level of precision for the present work.

A number of lines from the $\lambda\lambda$4250–4315 spectra are displayed in Figure 1 (lines of Cr), Figure 2 (Fe), and Figure 3 (Ti). These are strong lines, most of which appear to be relatively free from blending and may be suitable for modeling. Each row contains lines from one spectrogram, drawn on a horizontal scale that allows one to see the profile structure readily. Successive rows are observations at successive phases as listed in Table 1, starting with $\phi = 0.80$, the phase of negative field extremum, when the strong magnetic pole passes closest to the line of sight. The wavelength scale of the figures is heliocentric. Superposed on the observations are some calculated profiles. These will be described in § IV.

III. THE LINE SYNTHESIS PROGRAM

a) Program Structure

The program used to calculate the integrated intensity and polarization profiles of spectral lines for an assumed model atmosphere structure, abundance distribution, and magnetic field geometry makes liberal use of techniques and approximations devised for earlier similar line synthesis programs, most of which were developed for solar line profile studies. Since several extensive reviews of the construction of such programs have appeared (Stenflo 1971; Wittmann 1974, 1977; Hardorp, Shore, and Wittmann 1976; Landi Degl' Innocenti 1976; Martin and Wickramasinghe 1979), it will not be necessary to describe the present program in exhaustive detail. However, because of its central importance in the present investigation, some description must be given of the physical and mathematical assumptions, organization, and testing of the program.

The basic task that the line profile synthesis program must carry out is to calculate at a number of representative points on the visible hemisphere of a model star the local intensity and polarization profiles of one or several spectral lines, taking into account the assumed distributions of relevant elements,

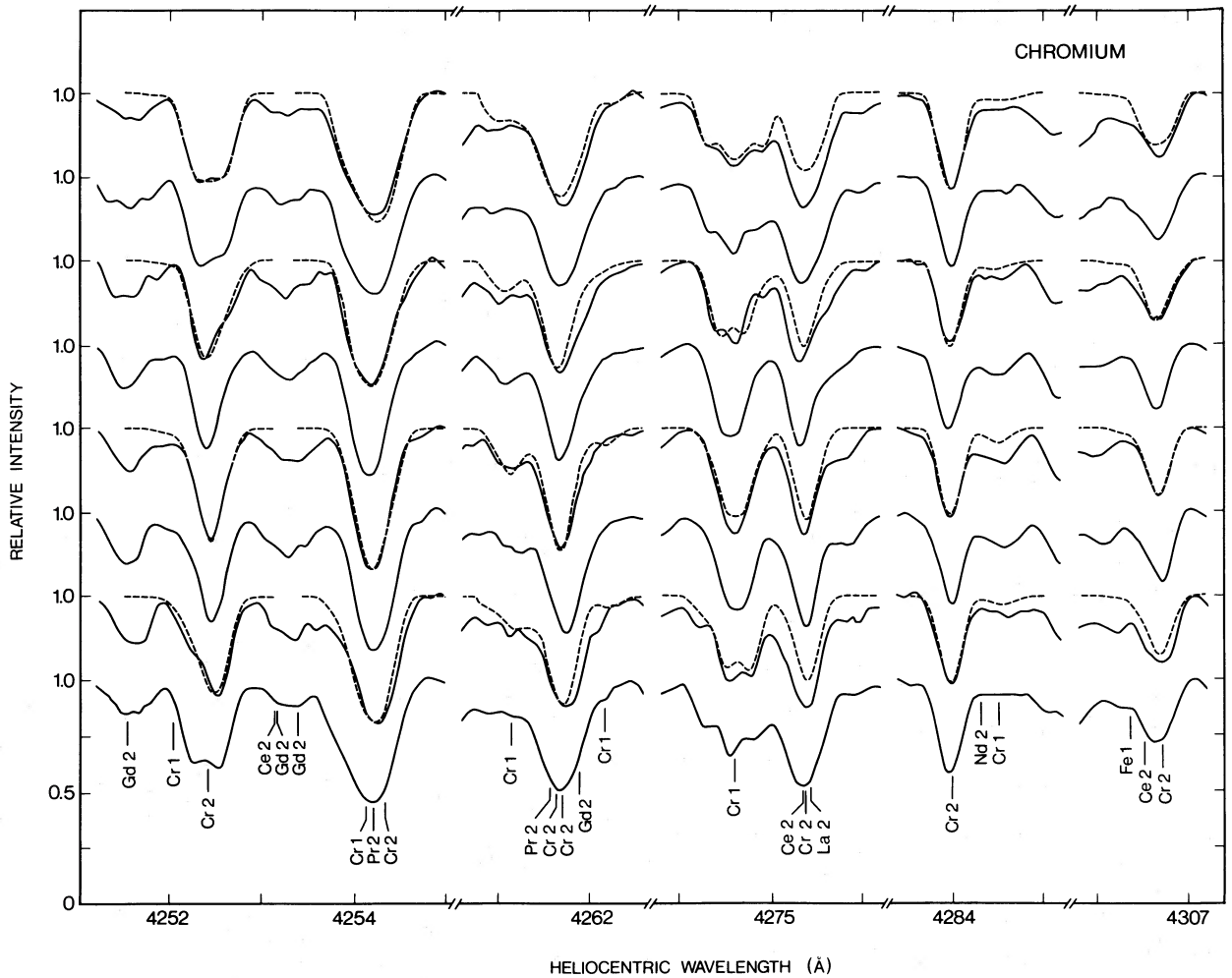

FIG. 1.—Observed profiles (*solid curves*) of several lines in the spectrum of 53 Cam that are primarily due to Cr. The eight rows are eight successive phases of the rotation of the star (see Table 1) starting with $\phi = 0.798$ when the strong negative pole is close to the line of sight. Identifications of contributing lines are shown below the bottom spectrum. Dashed curves are models computed as described in the text.

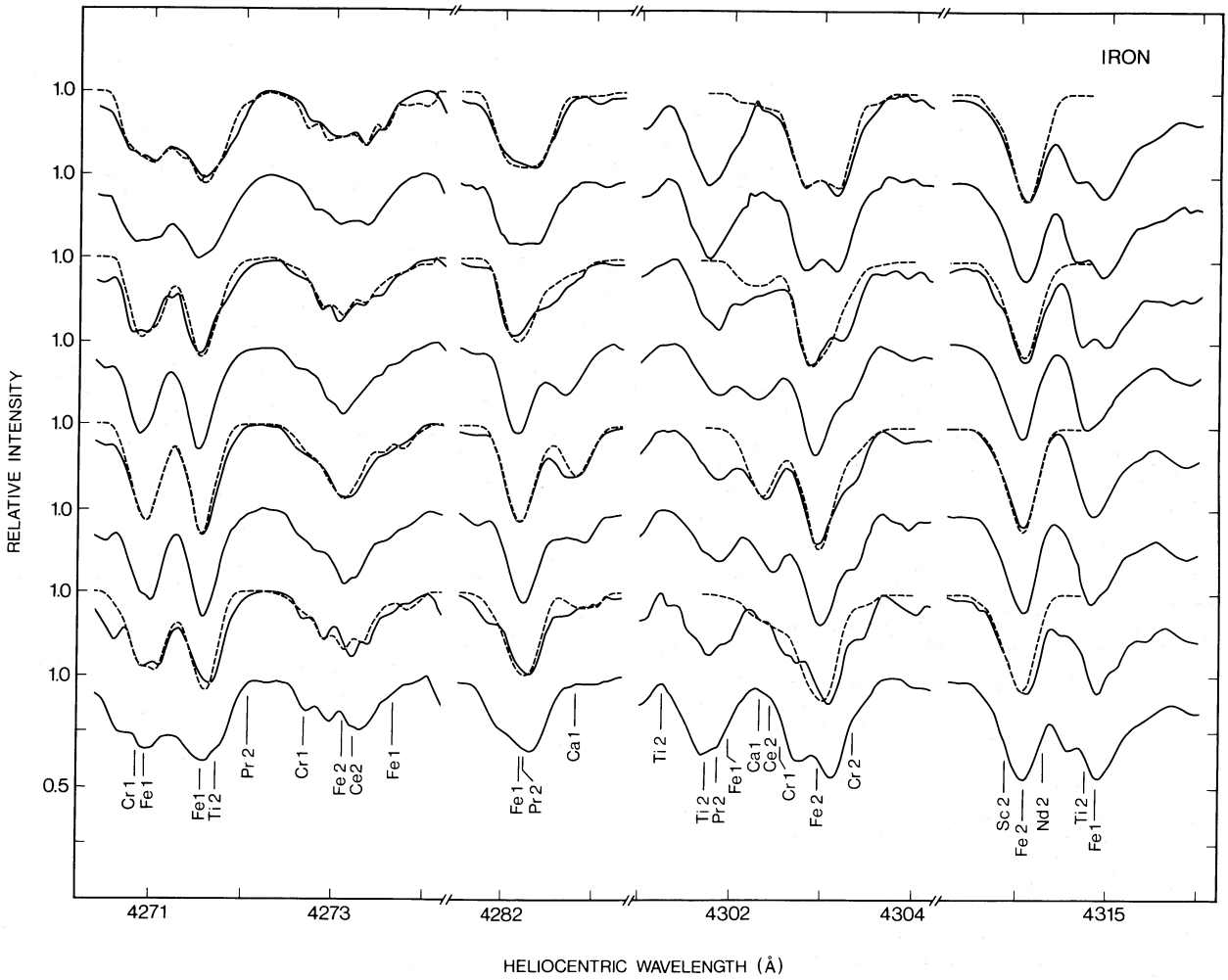

FIG. 2.—Same as Fig. 1, for lines due to Fe. The Ca lines at 4283 and 4302 Å and the Sc line at 4314 Å were also modeled.

the Zeeman splitting by the magnetic field, and the transfer of polarized light outward through the atmosphere. The local profiles must then be summed over the stellar disk with appropriate rotational Doppler shifts and instrumental profile to yield the theoretical profile for comparison with observation.

Calculation of a synthetic line profile for a particular star begins with the choice of a suitable model atmosphere. I do not calculate my own atmosphere models, but use the useful grids published by Kurucz (1979) for normal stars and by Muthsam (1978, 1979) for Ap and Bp stars. Justification for using atmosphere models calculated in normal hydrostatic equilibrium, ignoring magnetic forces, is discussed by Landstreet (1987). For 53 Cam, the calculated colors of Muthsam's model S76 ($T_e = 8500$ K, $\log g = 4.0$) are almost identical to the observed colors of the star, and this model has been used for almost all the line synthesis described in this paper. The fact that abundances derived using lines of neutral and ionized iron are very similar (see below) suggests that this atmosphere is an appropriate choice. However, Muthsam's models as tabulated do not contain all the information needed for the line synthesis calculation. In particular, the continuum optical depth scale τ_λ and the continuum opacity κ_λ at the wavelength λ of interest are needed. These are calculated from the reference continuum optical depth scale τ_0 at 5000 Å that is tabulated with the model, by computing at each level the continuum opacity $\bar{\kappa}_\lambda$ at λ and $\bar{\kappa}_0$ at 5000 Å due to bound-free and free-free transitions of neutral hydrogen and of the negative hydrogen ion, and to electron scattering (which is treated as a pure absorption process). Bound-free Gaunt factors for neutral H were taken from Carbon and Gingerich (1969), and the opacity of the negative H iron was computed with the polynomial fits given by Gingerich (1964). Then at each atmosphere level m, the optical depth scale at λ is computed using the approximation

$$\tau_\lambda(m) = \{[\bar{\kappa}_\lambda(m) + \tilde{\kappa}_\lambda(m-1)]/[\bar{\kappa}_0(m) + \tilde{\kappa}_0(m-1)]\} \times [\tau_0(m) - \tau_0(m-1)] + \tau_\lambda(m-1) . \quad (2)$$

A final opacity κ_λ more nearly consistent with that assumed in the construction of the model atmosphere than $\tilde{\kappa}_\lambda$ is then calculated from

$$\kappa_\lambda(m) = \{[\tau_\lambda(m+1) - \tau_\lambda(m-1)]/[d(m+1) - d(m-1)]\} , \quad (3)$$

where $d(m)$ is the geometrical depth of level m relative to an arbitrary reference level. This procedure was adopted because attempts to reproduce Muthsam's τ_0 scale directly using only

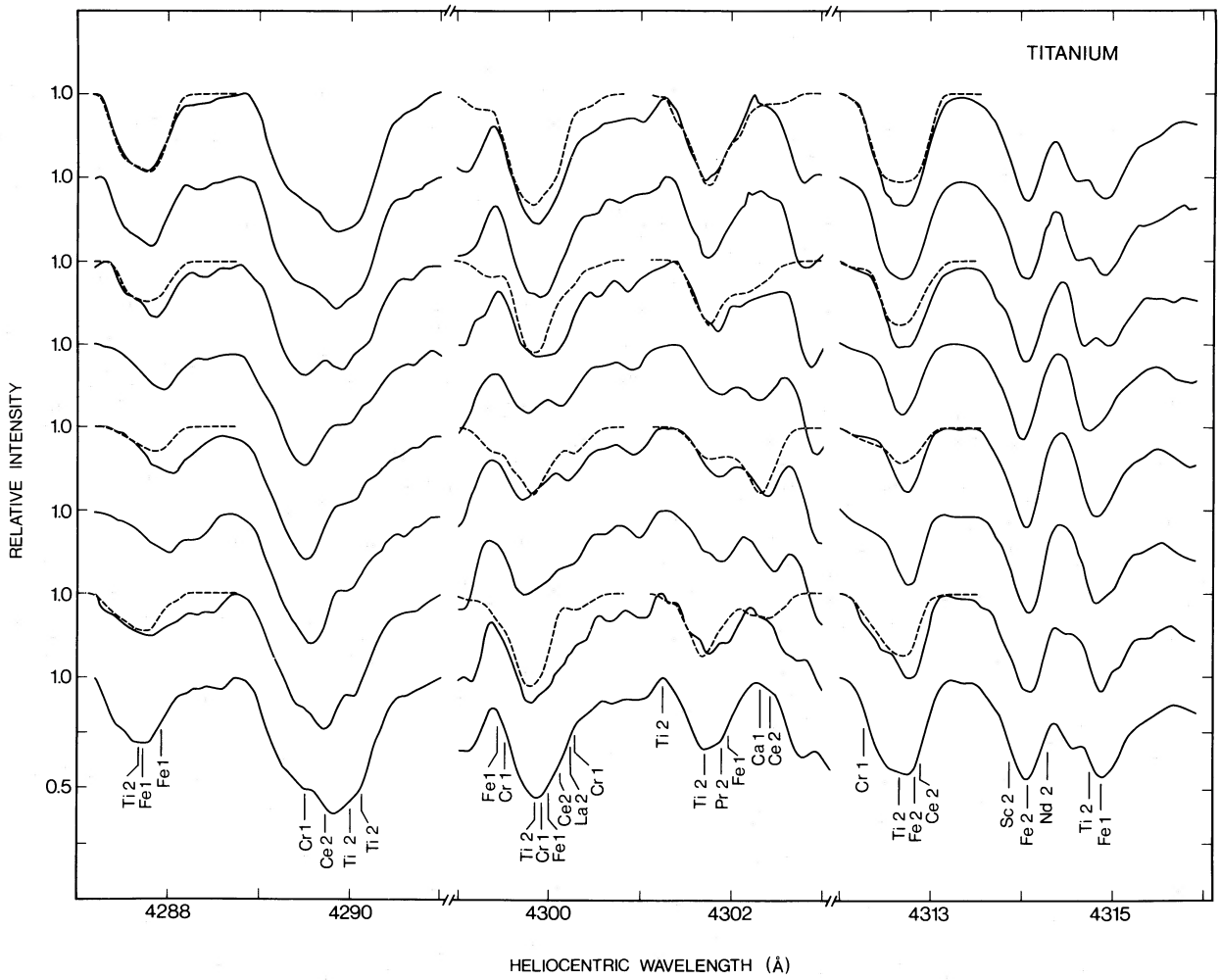

FIG. 3.—Same as Fig. 1, for lines due to Ti

the opacity sources listed above consistently resulted in τ_0 values that were 5%–30% lower than the tabulated values. Expressions (2) and (3) do not completely remove this problem, but they tie the optical depth scale τ_λ more closely to the tabulated τ_0 scale, especially for λ values not far removed from 5000 Å.

The spectral region synthesized is usually 2 Å wide. Synthesizing even such a small spectral region is quite costly in computer time (one model line at one phase requires typically 1000 s of CPU time on the Control Data Corporation Cyber 170/835 used for most of the calculations), and so the region synthesized is chosen to be just large enough to cover completely one line (or two with overlapping wings) of moderate strength. A model can be calculated for a single line if it appears to be reasonably free of blending, or it is possible to include a number of lines in the window, so that the importance of blends can be established. The Zeeman splitting pattern and relative strengths of the π and σ components of each line are calculated under the assumption of *LS* coupling, using *LS* quantum numbers from the Revised Multiplet Table (Moore 1945) or Atomic Energy Levels (Moore 1949), together with the appropriate equations as given by Condon and Shortley (1935, pp. 378–388). The assumption of *LS* coupling as an appropriate approximation for calculating the splitting of the dominant spectral lines modeled was tested by comparing the available observed Lande g-values for the upper and lower levels (Moore 1949) with those calculated in *LS* coupling; the experimental and theoretical g-values agree to within ± 0.02 for Cr transitions, ± 0.04 for Ti, and ± 0.05 for Fe.

Next the distribution over ionization states is calculated using the Saha equation for each of the elements represented in the line list to be synthesized, at each tabulated level of the model atmosphere. Partition functions are approximated by the polynomial approximations of Bolton (1970, 1971) and Aller and Everett (1972), except for ionization states for which no partition function data are available; in this case, the partition function is set equal to the ground-state multiplicity g_0. The line-to-continuum opacity ratio is calculated for the center of each line for a specified abundance, ignoring the effect of the field in splitting the line. This ratio is later corrected to the local abundance at various points on the disk, and the opacity is distributed appropriately among the various π and σ components of each line. Finally, damping constants are calculated for each line at all atmosphere levels. The radiation damping constants have been calculated for some of the stronger lines explicitly, using the gf-values of Kurucz and Peytremann (1975), including spontaneous emission as well as absorptions and stimulated emissions (Aller 1963, eq. [4-116]). For the

remaining lines, the classical damping constant is used. The collisional damping constant due to collisions with neutral H is computed using the Unsöld approximation for van der Waals broadening (Aller 1963, art. 7-5) or the tables of Deridder and van Rensbergen (1976), choosing the theory that yields the larger damping constant. Collisional damping by neutral He is neglected, since the abundance of He in Ap star atmospheres is believed to be abnormally low. Collisional damping by electrons is treated by the approximations given by Cowley (1971) for both neutral and ionized species.

The geometry of the magnetic field and of the abundance distribution of any nonuniformly distributed elements must be specified. The philosophy followed here has been to adopt physically reasonable geometries suggested by observation or theory that may be specified by a rather small number of parameters, and then to explore whether a more-or-less unique region in parameter space can be found that leads to calculated line profiles that are in reasonable agreement with those observed through the rotation cycle for a variety of spectral lines of differing strengths and Zeeman splitting patterns. The magnetic field geometry used for these calculations is axisymmetric and may include a superposition of dipole, linear quadrupole, and linear octupole fields (Panofsky and Phillips 1955). Alternatively, the dipole component can be decentered along its axis. The parameters required to specify the magnetic geometry are the inclination β of the field axis to the rotation axis, the polar field strengths B_d, B_q, and B_0 of the multipole components, and the decentering a of the dipole along its axis as a fraction of the stellar radius. (When a model with a decentered dipole is calculated, the polar field strength is specified for the same dipole field centered.) The abundance distributions used for 53 Cam are also assumed to be axisymmetric about the magnetic field axis, an arrangement that is physically consistent with the view that the nonuniform atmospheric abundance distributions are due primarily to the effects of the magnetic field (Vauclair, Hardorp, and Peterson 1979; MMC). The assumed distribution consists of one or two rings (or caps) of uniform abundance ϵ_1 and ϵ_2, where $\epsilon_Z = n_Z/n_{\rm tot}$, and a background abundance ϵ_b that applies outside the rings. For each ring we must specify the range in α, the colatitude measured from the stronger magnetic pole, over which the ring extends. Finally, the inclination i of the stellar rotation axis to the line of sight must be specified, as must the assumed value of $v \sin i$ (actually a small grid of $v \sin i$ is calculated for each model), and the rotational phase of the star.

Having done the preliminary computations, the program turns to calculating the local intensity and polarization line profiles at a number of points on the disk, and then summing these profiles appropriately to produce the integrated line profile that is to be compared with observation. The stellar disk is divided into a number $i_{\rm tot}$ (usually four) of concentric rings of equal projected radial width. Each ring is in turn divided into $6i$ equal sectors, where i is the ordinal number of the ring counting out from the center. This produces a division of the visible hemisphere of the star into $3i_{\rm tot}(i_{\rm tot} + 1)$ compact integration areas of roughly equal projected areas.

At each sampled disk point, the program calculates the angular distance α from the strong magnetic pole and the x, y, and z components of the local magnetic field in the observer's frame of reference, which has the z-axis parallel to the line of sight and the stellar rotation axis in the x-z plane. The field strength is then used to compute, using the previously calculated Zeeman splitting pattern, the local wavelength positions of the various line components of a single spectral line. For each component, the local ratio of line-to-continuum opacity at component center is evaluated using the ratio previously calculated for a reference abundance value, the computed relative strengths of the individual components, and the local abundance. This calculation is repeated for all the spectral lines included in the window being synthesized.

The next (and most expensive) step is to integrate the coupled equations of tranfer that describe the emission of polarized light (Unno 1956; Wittmann 1974; Hardorp, Shore, and Wittmann 1976) out through the atmosphere at the sampled disk point for a number of wavelengths in the wavelength window being synthesized. For the calculations reported here, this is done in the approximation that anomalous dispersion is neglected. For this computation, it is necessary to evaluate the polarized ratios of line-to-continuum opacity η_I, η_Q, and η_V, which refer, respectively, to the I, Q, and V components of the Stokes vector describing radiation propagating along the line of sight, as a function of wavelength through the window to be synthesized. Because the thermal Doppler dispersion is only $\sim$0.03 Å for spectral lines of iron peak elements, the line-to-continuum opacity ratios are sampled at intervals of 0.01 Å. The opacity ratios for each spectral line included in the window are calculated using the numerical algorithms for Voigt profile calculation described by Baschek and Scholz (1982, § 4.3.4., eq. [111]). Microturbulence is assumed to be suppressed by the strong magnetic field and is set equal to zero. The opacity ratios are summed over all the lines to yield total opacity ratios η_I, η_Q, and η_V as functions of wavelength. This must be repeated for all tabulated levels in the model atmosphere used.

To numerically integrate the equations of transfer, I make use of the very efficient technique proposed by Martin and Wickramasinghe (1979), in which the coupled equations of transfer are treated as having constant coefficients between one tabulated atmospheric depth and the next, so that the analytical solution described Unno (1956) may be used to calculate at depth m in the atmosphere the values of the components of the Stokes vector from the values at depth $m + 1$. The coefficients of the equations are taken to be the averages of their values at levels $m + 1$ and m. The equation of transfer is integrated outward from the shallowest layer in the atmosphere for which τ_λ exceeds 10. The inner boundary condition with which the integration is started is the assumption that radiation field at the initial level of the integration is unpolarized blackbody radiation. It has been shown by Martin and Wickramasinghe (1979) that this technique is essentially as accurate as, and much faster than, the usual direct numerical integration using a Runge-Kutta method.

The integration routine was implemented essentially as described by Martin and Wickramasinghe (1979) in their equations (14)–(26), with one exception. To reduce computing time, the far wings of each line component are cut off where the line-to-continuum ratio for that component drops below $\sim 10^{-3}$. This can lead to the situation that both η_Q and η_V vanish at some levels of the atmosphere, which causes a number of expressions in Martin and Wickramasinghe to be undefined. This is not simply the problem of transfer in a completely unpolarized continuum, for which the normal solution to the equation of transfer applies, since absorption in line wings at greater depth than the level in question may lead to emergent polarization (i.e. a nonzero value of Q or U) trying to make its way out through a nonpolarizing atmosphere. In this

case, the equations of transfer (in the usual notation) become

$$\mu\, dI/dt = \eta(I - B)\,, \tag{4}$$

$$\mu\, dQ/dt = \eta Q\,, \tag{5}$$

and

$$\mu\, dV/dt = \eta V\,, \tag{6}$$

where $\eta = \eta_I$. Since the equations are now fully uncoupled, the solution for a single first-order differential equation with constant coefficients may be used between one level and the next for each, and in the notation of Martin and Wickramasinghe the values of the components of the Stokes vector at level m are related to those in the (next deeper) level n by

$$I_m = B_n + (I_n - B_n)\exp\left[-\eta(\tau_n - \tau_m)/\mu\right] + (\mu\gamma/\eta)\{1 - \exp\left[-\eta(\tau_n - \tau_m)/\mu\right]\}\,, \tag{7}$$

$$Q_m = Q_n \exp\left[-\eta(\tau_n - \tau_m)/\mu\right]\,, \tag{8}$$

and

$$V_m = V_n \exp\left[-\eta(\tau_n - \tau_m)/\mu\right]\,. \tag{9}$$

This solution also applies, of course, in the continuum where the inner boundary condition specifies $Q = V = 0$ at the deepest level. The value of the emergent unpolarized continuum flux is calculated once for each integration ring for normalization purposes.

After the emergent values of the I, Q, and V components of the Stokes vector have been calculated as a function of wavelength for a single integration point on the stellar disk, the Q component must be transformed from the reference frame of the computation, in which the U component is zero, to the reference frame of the star as a whole, in which both Q and U are in general not zero. Then the program sums all the local components of the Stokes vector, each weighted by the area of projected disk which it samples, with appropriate Doppler shifts as required by the assumed value of $v \sin i$.

Finally, the calculated profile is broadened by convolution with a spectrograph profile of FWHM = 0.10 Å. This has the effect of smoothing out fine-scale ripple due to the rather coarse gridding of the observed stellar hemisphere.

b) *Program Testing*

In a program such as this one, constructed *ab initio* and containing of the order of 1000 FORTRAN statements, the possibility of programming or mathematical errors is very real, and testing is an important consideration. Because the program is mainly constructed of subroutines, it was relatively easy to test individual program segments for correct operation. This was done extensively; a few examples will indicate the kind of testing carried out.

The subroutine that calculates continuum opacities for use in transforming to the optical depth scale at the wavelength of interest was used to produce opacity tables that could be compared to reference opacities calculated by Carbon and Gingerich (1969). Agreement was achieved to within ~4%; the observed differences are believed to be due to small differences in the values of physical constants, a slightly different treatment of high-level terms in the bound-free opacity of hydrogen, and the fact that my opacity calculation ignore continuum opacity due to such sources as C, Mg, and Si.

The subroutine that calculates Zeeman splitting (displacement and relative strengths of line components) was tested by comparison with several examples given in Condon and Shortley (1935, pp. 382–383) and Beckers (1969). Calculation of the magnetic field strength and orientation for given field configurations seen in the observer's frame of reference was tested by choosing points on the star in a variety of geometrically simple orientations in which the computed result could be easily verified.

Testing of the routine for integrating the equations of transfer is particularly important, since errors in this subroutine do not necessarily produce output that looks unreasonable. The most demanding test carried out on this subroutine was to verify that it reproduces to high accuracy the analytical solution to the equations described by Unno (1956) when the line-to-continuum ratios η_I, η_Q, and η_V are artificially forced to be constant with depth in the star, and the source function is forced to be linear in optical depth τ_λ. Another kind of test carried out was to investigate the convergence of the solution. Experiments showed that as long as the outward integration is started deeper in the atmosphere than about an optical depth $\tau_\lambda = 7$, the surface results are independent of the depth at which integration is started. Similarly, experiments were run in which the integration connected only every other level, every third level, etc. As the number of atmosphere levels included in the integration increases, a clear convergence to the solution using all levels is found; the emergent intensity and polarization for a single ray in a solution calculated using every other level rarely differ from the result using all tabulated levels by as much as 3%. Profiles were also calculated using more and fewer sampling, points on the disk; it was found that with four rings (60 points) the line profiles are quite close to the profiles calculated with much finer gridding.

Finally, the overall operation of the program was checked in the nonmagnetic limit by calculating equivalent widths of a number of solar spectral lines studied by Blackwell and Shallis (1979). Using the same model atmosphere, atomic constants, and abundances, the present program reproduces the equivalent widths calculated by Blackwell and Shallis to within a few percent.

IV. A MODEL FOR 53 CAM

a) *Magnetic Field Geometry*

i) *Previous Magnetic Models*

Previous discussions of magnetic field geometries have generally made the connection between theoretical models and observation by means of various averages of the field distribution over the visible stellar hemisphere, such as the effective field B_e (the line-of-sight component of the field averaged over the visible hemisphere, weighted by limb darkening) and the mean surface field B_s (the average scalar magnitude of the field, weighted by limb darkening). These moments of the field distribution are easily calculated for theoretical models (e.g. Schwarzschild 1950). On the observational side, various types of observations can be interpreted as providing measurements of these moments. For example, Babcock (1958) argues that the separation of the centroids of a spectral line as viewed in right and left circularly polarized light is proportional to the effective field present. This result has provided the basis for the interpretation of essentially all the photographic measurements of magnetic fields by Babcock, Preston, and others. More recently, Landstreet (1982) has shown that in the case of a weak magnetic field in a star in which the source function depends linearly on optical depth and in which the line-to-continuum opacity ratios (the η's of § III) are independent of

depth, the measured circular polarization in the wings of a Zeeman triplet is directly proportional to the mean line-of-sight component of the field weighted as cos θ, where θ is the angle between the line of sight and the local radius vector. This particular moment of the field may be approximately what is measured using the Hβ Zeeman analyzer. It is similar to but not the same as the effective field, and has been termed the mean longitudinal field, B_l. The mean surface field was introduced by Preston (1970, 1971*b*), who argued that it may be measured by the excess line widening due to the Zeeman effect.

Measurements of all of these field moments as functions of phase have been reported in the literature for 53 Cam, and from previous modeling efforts a fairly definite starting model is available. Babcock (1960) reported the existence of a large effective field in this star, and showed that the field as measured photographically varies periodically but rather anharmonically with a period of 8.03 days between extrema of about -5200 and $+3600$ G. Böhm-Vitense (1965) found that the photographic magnetic field observations of this star cannot be modeled by a dipole field, but she was unable to find a magnetic configuration that reproduces the observed photographic magnetic curve. Landstreet (1970) showed that the observations of the star cannot be modeled by any field configuration that is antisymmetric through the magnetic equator, and proposed that the star has one magnetic pole that is stronger than the other. A model of this star having the geometry of a dipole decentered along its axis by a very large amount (0.67 stellar radius) was shown to be able to reproduce the observed photographic field measurements, assuming that they actually measure the effective field. Shortly afterward, following on Preston's (1969*b*) discovery that some spectral lines of 53 Cam exhibit obvious magnetic splitting for part of its rotation cycle, Huchra (1972) made measurements of the mean surface field of the star. These measurements show a surface field that increases monotonically from a low value of ~ 10 kG at the positive effective field extremum to a maximum of 17 kG at the negative field extremum. This behavior is consistent with Landstreet's proposal that the star has a strong pole and a weak pole, but the actual surface field variation observed has a much smaller amplitude than was predicted by Landstreet's model. Huchra proposed a model based on the decentered dipole distribution that correctly predicted the observed extrema of both the effective and surface fields with a much smaller decentering (~ 0.145 stellar radius toward the negative pole), but his model does not correctly predict the shape of the photographically observed effective magnetic field variation as a function of phase.

The resolution of this problem was suggested by Borra (1974), who argued that the magnetic field curve as measured by the standard photographic method is not simply related to the effective field curve that would be predicted by a correct model of the field distribution. Borra's suggestion was followed up by Borra and Landstreet (1977), who measured the effective field variation of 53 Cam photoelectrically using the circular polarization produced in the wings of Hβ by the Zeeman effect. The new observed effective field curve, which has field extrema of $+4200$ and -5400 G, is much more sinusoidal than that obtained from photographic measurements, and a model very similar to the one suggested by Huchra was found to reproduce reasonably well both effective and surface field measurements. The model adopted by Borra and Landstreet is a dipole decentered toward the strong negative pole by $a = 0.15$ stellar radius, with a polar field $B_d = 17{,}200$ G at both poles before decentering, corresponding to actual polar field strengths of $-28{,}000$ and 11,300 G at the negative and positive poles, respectively. On this model, the inclination i of the rotation axis and the obliquity β of the magnetic axis with respect to the rotation axis are 65° and 80° (it is not possible from the data described above to determine which value refers to i and which to β), with the strong negative pole passing within $\sim 15°$ of the line of sight at negative effective field extremum, and the positive pole passing $\sim 35°$ from the line of sight. Thus during the rotation period of the star, the line-of-sight surveys the field almost from one pole to the other. This is a particularly favorable circumstance for modeling.

ii) *Choice of Appropriate Magnetic Model*

For values of the decentering of less than ~ 0.3 stellar radii, the centered dipole may be fairly accurately represented by the sum of a dipole plus a parallel linear quadrupole, both located at the center of the star. The equivalence of these two representations of the field up to first order in the decentering parameter a has been demonstrated by Deridder, van Rensbergen, and Hensberge (1979). They show that if one defines $q = B_q/B_d$, where B_q is the polar strength of the quadrupole component, then the relationship between the two types of models is given by $q = 3a$. Thus for 53 Cam, we could start with a dipole plus quadrupole model in which the quadrupole has a polar strength of ~ 0.45 of that of the dipole, in close agreement with the model discussed by MMC. There are two reasons for raising this possibility. One is that MMC have argued that magnetic stars may have field distributions that are in fact better represented by the dipole plus quadrupole configuration rather than by the decentered dipole, and have shown that if q is greater than one, the effects of the field on horizontal diffusion of elements may be quite different for a dipole plus quadrupole than for a comparable decentered dipole. (I shall address below the question of whether one can distinguish these two models observationally in the case of 53 Cam.) The other reason for introducing the dipole plus quadrupole model is that if the decentered dipole model is found to be unable to reproduce observations well, one has no natural next step. In contrast, the dipole and quadrupole are simply the first two terms of an expansion of the field distribution in (axisymmetric) multipoles, so that a natural generalization of the model is readily available.

The observed effective and surface magnetic field curves of 53 Cam are quite symmetric to reflections around the phases of their extrema. As discussed by Landstreet (1970), this indicates that it should be possible to model the magnetic field geometry with a field distribution that is axisymmetric. Any arbitrary static, curl-free axisymmetric magnetic field distribution may be represented as a superposition of multipoles, and as it seems likely that we shall only be able to determine the large-scale structure of the field, it is reasonable to restrict the allowed field geometry to dipole, quadrupole, and octopole terms. For such a model it is necessary to specify the polar field strength (B_d, B_q, B_o) of each multipole, as well as the inclination i of the stellar rotation axis to the line of sight, and the obliquity β of the field axis to the rotation axis. To make comparison with observation, one must of course also specify either the projected rotation velocity or (equivalently) the stellar radius.

Comparison of the magnetic field model with the available spectra of 53 Cam is fairly straightforward with the use of the line synthesis program described in the preceding section. In

principle, one may calculate the profile of any line that is reasonably sensitive to Zeeman splitting, and compare the calculated profiles to those observed at a variety of phases. In practice, this process is complicated by two factors. First, because the radius of the star is not at all well known, the value of $v \sin i$ cannot be calculated in advance, and so for a single spectral line one does not know how much of the broadening to attribute to the field and how much to attribute to rotation. This problem may be resolved, and $v \sin i$ determined, by synthesis of two lines of greatly different Zeeman splitting properties. Second, the calculated profile will depend on the assumed abundance distribution, and so the field cannot be determined without considering at the same time the abundance problem. In 53 Cam, it is found that the abundance of Cr is fairly uniform over the stellar surface, and it is possible to determine the field geometry reasonably unambiguously from lines of this element alone, so that when the abundance distribution of other, more nonuniformly distributed elements is considered later, the field may be considered to be already established.

At present, comparison of the magnetic model with the Hβ polarization observations, which constrain the line-of-sight component of the field, is in a much less satisfactory state. In principle, one should calculate Hβ line intensity and circular polarization profiles for comparison with the observations. However, my line synthesis program cannot yet calculate Balmer line profiles, which (*a*) requiree a different formulation of the absorption coefficient in the wings than do the metal lines, (*b*) may exhibit Paschen-Back rather than normal Zeeman splitting in the fields of interest in 53 Cam, and (*c*) require a much larger wavelength window than most metal lines. Thus, for the present, I am still forced to regard the Balmer line data as constraining some kind of effective field moment of the model field distribution. From the analytical results of Landstreet (1982) discussed above, it is tempting to interpret the Balmer line observations as providing measurements of the longitudinal field B_l. However, numerical experiments with synthesizing artificial strong lines in specified field distributions suggest that the line wing circular polarization produced by the field is not quite as large as that expected from the usual relationship between field strength,

$$(V/I) = 4.67 \times 10^{-13} B\lambda^2 (dI/d\lambda)/I \qquad (10)$$

(Landstreet 1982), on the assumption that B is the longitudinal field, but is slightly larger than that expected assuming that B is the effective field of the assumed field distribution. In view of this situation, in the present modeling work I shall simply assume that the Balmer line measurements measure the effective field. This probably leads to errors comparable in size to those due to the scale uncertainty of the Hβ magnetic measurements caused by imprecise measurement of the line profile, $\sim$10%–20%.

In addition to a definite means of comparing the model field distribution to the available data, we also need a correction procedure that may be applied to force successive versions of the model to conform increasingly closely to the observations. The field moments B_e and B_s are very useful for this purpose, as specification of the values of these moments at magnetic extrema is sufficient to allow determination of the model parameters B_d, B_q (or a), i, and β, apart from the ambiguity of a possible interchange of i and β. A suitable method for determining the model field parameters from the observed moments is described by Preston (1970). As discussed above, the B_e values are assumed to be provided directly by the Balmer line magnetic observations, and the extreme values are held constant. The values of B_s at the field extrema are not now derived from the observations by the procedure described by Preston (1970), but are treated as parameters that are to be adjusted to bring the widths of the computed line profiles into better agreement with the observed lines at the appropriate rotational phases. The utility of this procedure comes from the fact that an increase (decrease) in B_s at one of the field extrema is always found to result in an increase (decrease) of the line width at that phase by an amount that may be adjusted in only a couple of interations to fit the observations.

iii) *Determining Magnetic Model Parameters of 53 Cam*

In the $\lambda\lambda$4250–4315 region, the λ4284 line of Cr II is the least magnetically broadened of all the reasonably strong lines. At maximum B_s, this line is quite obviously the narrowest line in the spectrum. In fact, the profile hardly changes at all through the rotation period of the star (see Fig. 1). This not only indicates the small sensitivity of this line to magnetic splitting, but also strongly suggests that the global Cr distribution over the surface of 53 Cam is approximately uniform. Furthermore, a number of reasonably strong Cr I and Cr II lines are visible in the spectrum, which have a fairly wide range of Zeeman patterns. For these reasons, the first attempts to test the magnetic model were made by calculating line profiles of the lines λ4254 ($z = 1.38$) and λ4274 ($z = 1.96$) of multiplet 1 of Cr I, and the lines λ4252 ($z = 1.20$), λ4275 ($z = 0.90$), and λ4284 ($z = 0.50$) of multiplet 31 of Cr II, at the phases of magnetic extrema, $\phi = 0.30$ and 0.80, assuming that Cr is uniformly distributed. Comparison of calculated profiles of λ4284 with those observed established that the value of $v \sin i$ is 13 ± 1.5 km s^{-1} and the stellar radial velocity is -15 ± 2 km s^{-1} for all spectra. Observed profiles of $\lambda\lambda$4252 and 4284 at phases of field extrema could be reproduced reasonably well, although the calculated profile of λ4252 was a bit wider than the observed line at the negative extremum. The shape of λ4274 could also be reproduced qualitatively with this model, although again the model line was slightly too wide at the negative extremum. Neither λ4254 nor λ4275 could be reproduced at all accurately on this first exploration; it subsequently became clear that both are blended, and they were not used further to determine the magnetic model.

The excess widths of the computed lines $\lambda\lambda$4252 and 4274 at negative extremum suggested that the surface field at the negative pole was slightly too large. Reduction of the surface field at $\phi = 0.80$ by $\sim$10% led to a new model, characterized by a dipolar field strength at the pole before decentering of $B_d = -16{,}100$ G (the sign is appropriate for the stronger magnetic pole), a decentering parameter $a = 0.10$, and i and β values of 72° and 75°. The corresponding field moments at the negative and positive field extrema, assuming a limb darkening coefficient of 0.575 [determined from the variation of $I_\nu(\theta)$ in the continuum from calculations with the line synthesis program] are $B_e^- = -5480$ G, $B_s^- = 15{,}730$ G, $B_e^+ = 4320$ G, and $B_s^+ = 10{,}290$ G. The variation of B_e and B_s as functions of α (the colatitude measured from the strong magnetic pole) for this model, and for others discussed below, are shown in Figure 4. This model gives quite satisfactory fits to both λ4252 and λ4284 at the phases of field extrema, and a calculated profile of about the right width (but not the correct shape) for λ4274. However, calculated profiles of both $\lambda\lambda$4252 and 4274 at phases 0.05 and 0.55, when the effective field is passing through zero and the line of sight to the center of the star passes nearly

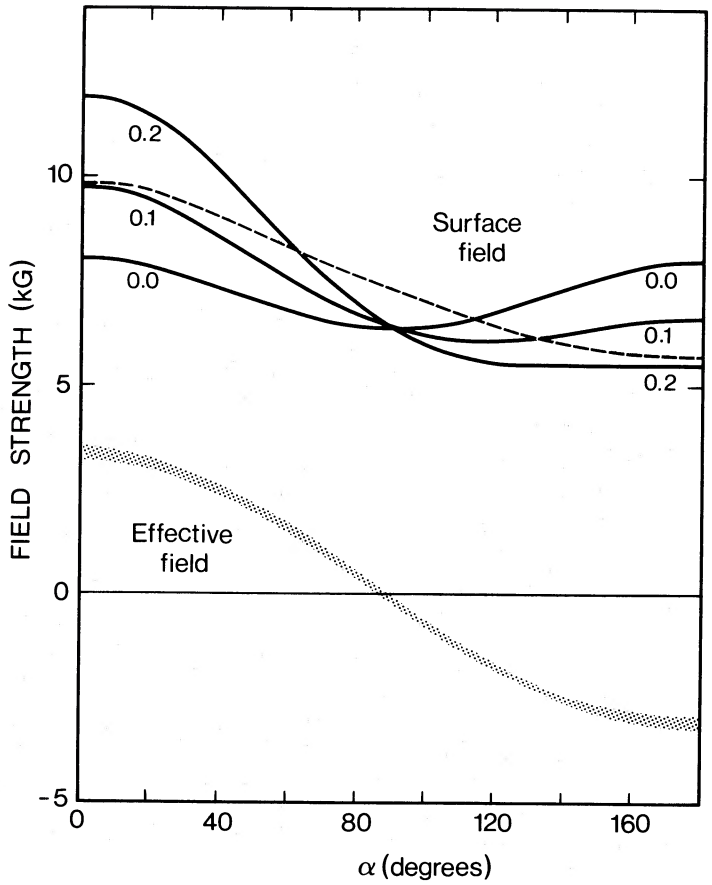

FIG. 4.—Variation of effective field B_e and surface field B_s as functions of colatitude α from the strong magnetic pole is shown for centered ($a = 0$) and decentered dipole ($a = 0.1$, 0.2) models. The variation of a dipole-quadrupole model with $q = B_q/B_d = 0.3$ is almost indistinguishable on this scale from that of the $a = 0.1$ decentered dipole. A model having $B_d/B_q/B_o = 1.0/0.48/-0.30$, the same ratio adopted for the final model of 53 Cam, is shown as a dashed line; note that B_s for this model near $\alpha = 90°$ is not at a local minimum, in contrast to the other models. All the models are normalized to a (centered) polar dipole field strength of 10 kG. The B_e cuves are all very similar to one another and are shown as one broad shaded curve.

through the magnetic equator, were found to be considerably narrower than the observed profiles.

The origin of this problem is the fact that a decentered dipole field of moderate decentering (or the equivalent dipole-quadrupole field) has a minimum value of B_s for $\alpha \sim 90°$, where B_e is near zero (see Fig. 4). Even for $a = 0.20$ the value of B_s near $\alpha = 90°$ is no larger than that observed over the weak pole. The width of the line when $B_e \sim 0$ cannot be adjusted by changing the parameters of the model, since these are completely determined (except for interchange of i and β) by observations at B_e field extrema. The only means to improve agreement with observation is to add a further field component to the model. A linear octupole aligned with the dipole adds only one more parameter to the magnetic field geometry, and because the sign of the normal component of the field reverses in each hemisphere (compared to a dipole which has a constant radial component sign in each hemisphere), the octupole component may be chosen to reduce the dipole field near the poles while enhancing it near the equator. This is exactly the behavior needed.

For mathematical consistency at this point we change from a decentered dipole to a dipole-quadrupole model, now supplemented by an octupole. For any specified strength of the octupole component, the dipole and quadrupole polar field strengths, B_d and B_q, and the values of i and β may still be determined from the values of B_e^+, B_s^+, B_e^-, and B_s^-. Then for a family of models with values of B_d and B_a determined in this way, but various values of the octupole polar field B_o, comparison of the calculated line profiles with those observed near $B_e = 0$, determines the value of B_o. The best fit to the observations is found for the model with $B_d = -16{,}300$ G, $B_q = -7300$ G, and $B_o = +4900$ G. The corresponding values of i and β are 64° and 82° (or 82° and 64°). The quantities B_d and B_q are determined in this way to within $\sim 10\%$, and B_o to within $\sim 20\%$. The angles are determined to within a few degrees. The new model still yields a good fit to the line profiles at $\phi = 0.30$ and 0.80, and gives a much more satisfactory (although still not quite exact) fit near $\phi = 0.05$ and 0.55. This magnetic model is adopted throughout the remainder of this paper and will receive considerable testing as evaluation of the abundance distributions proceeds.

Note an important conclusion to emerge from fitting the magnetic field geometry: *the observational data contain enough information to reveal a shortcoming of the initial decentered dipole model and to define a more elaborate improved model reasonably uniquely.* However, the data are not able to discriminate between a decentered dipole and the corresponding dipole-quadrupole model. Figure 4 indicates that the variation of B_s and B_e with α of these two models is very similar, and synthesis of spectral lines with corresponding models leads to

line profiles that differ by less than 1% anywhere in the profile. However, a choice might be possible in a star having a larger ratio of B_q/B_d (e.g., HD 126515 = Preston's star; see MMC).

b) *Abundance Distribution of* Cr

From the line synthesis carried out to determine the magnetic field geometry, it is found that the best Cr lines may be modeled approximately using a constant abundance of Cr over the stellar surface, with an abundance (on the scale defined by the Kurucz-Peytreman oscillator strengths) of about $\epsilon_{Cr} = 1 \times 10^{-5}$. However, several points must be considered before a definitive abundance map is obtained. First, most lines in the spectral regions observed appear to be at least mildly blended, usually with weak lines of Fe-peak elements or with rare earth lines. Second, in view of the small wavelength window studied, it is important to use the best oscillator strengths available. Finally, small systematic differences between calculated and observed lines suggest that Cr may not be distributed quite uniformly, so we must experiment with some possible simple abundance geometries to see if a better distribution may be found.

Synthesis of Cr lines carried out while determining the magnetic field geometry strongly suggests that even many deep, apparently unblended lines in the spectrum of 53 Cam in fact contain significant blends. This is indicated by the fact that even when a few lines had been modeled very successfully, others were observed to be too strong, at the wrong radial velocity, too broad, or asymmetric when compared with the theoretical profiles. In most cases the problems could not be made to vanish simply by assuming that the oscillator strengths used were in error. Attempts to identify possible blends by examining the Revised Multiplet Table (Moore 1945) proved to be inconclusive because of the limited number of high-excitation lines tabulated and because of the lack of oscillator strengths. The much more extensive line list of Kurucz and Peytreman (1975) was more helpful, but very unwieldy due to the enormous number of lines tabulated (almost 2000 lines are listed in the printed version of the list in the spectral region $\lambda\lambda$4250–4315 alone). To use this list more systematically, a computer program was written by A. Sigut which reads in all the lines in the spectral region observed from a magnetic tape version of the Kurucz-Peytreman list, and calculates for each line a very approximate value of η_0, the line-to-continuum opacity ratio at line center. For this calculation, conditions appropriate to an optical depth of $\tau_\lambda \sim 0.3$ in the Muthsam atmosphere model used for 53 Cam are assumed, and the abundance table AB (appropriate to a rather extreme Ap star) of Muthsam (1979) was used. The output of this program is a list of only those spectral lines having η_0 greater than some chosen limiting value, typically 0.1. This selection dramatically reduced the line list to be considered for possible blending lines; in the $\lambda\lambda$4250–4315 region only $\sim$200 spectral lines are expected to contribute significantly to the observed spectrum. In addition, the rough relative strengths calculated greatly facilitated identification of the most important probable blends. This list of stronger lines was found to be extremely useful in identifying nearly unblended lines and in selecting likely blends to include in synthesis calculations.

The strong lines of Cr in the $\lambda\lambda$4250–4315 region are $\lambda\lambda$4254, 4274, and 4289 of multiplet 1 of Cr I, and the lines $\lambda\lambda$4252, 4261, 4269, 4275, and 4284 of multiplet 31 of Cr II. In addition, a high-excitation line of Cr II at 4306 Å (tabulated in the Kurucz-Peytreman list but not in the Revised Multiplet Table) appears to be fairly strong. Of the Cr I lines, λ4274 seems to be largely unblended, λ4254 is blended mainly with a comparably strong high-excitation line of Cr II, and λ4289 is blended with a strong and variable Ti II line. Calculations of Cr I lines were therefore largely restricted to λ4274, although some experiments were carried out on λ4254. Of the Cr II lines, $\lambda\lambda$4252 and 4284 seem to be almost unblended, so most calculations refer to these two lines. Some experiments were carried out on the λ4261 line, which is mildly blended with two other Cr lines, but it appears that this line contains further important blends, probably due to the rare earths Pr and Gd. Because almost none of the rare earths have clean lines in the available spectroscopic material, it was not possible to determine accurate abundance distributions for any of the rare earths, and so *rare earth blends were not included in any of the line synthesis calculations.* For this reason, some of the theoretical profiles in Figures 1–3 fall rather short of filling the observed profiles. Both the λ4269 line and the λ4275 were found to be badly blended, probably mainly by rare earth lines. The Cr lines for which some calculations were carried out are listed in Table 2, together with important blending contributors. Principal lines are denoted by footnote (a); rare earth lines that are probably important blend contributors, but that were not included in line models, are denoted by footnote (b).

Kurucz-Peytreman oscillator strengths (KP/K) are listed in Table 2 for all the lines for which they are available, as are the most accurate experimental values that I have been able to find ("Observed") with their sources ("Reference"). Most of the experimental *gf*-values for lines of neutral Fe-peak elements come from the critically evaluated compilations published by the group at the US National Bureau of Standards, or from recent work by the Oxford group. The experimental *gf*-values from these two sources are in general in reasonable agreement with the Kurucz-Peytreman values. When accurate experimental *gf*-values are available, I have generally used them in line synthesis calculations.

However, the only recent experimental *gf*-values for Cr II, due to Wujec and Weniger (1981), have not been critically evaluated by the NBS; furthermore, the experimental values are in dramatic disagreement with the Kurucz-Peytreman values, typically by a factor of more than 10. This discrepancy was serious enough that a program to obtain astrophysical *gf*-values has been started (Sigut and Landstreet 1988). Preliminary results suggest that the *relative gf*-values given by Kurucz and Peytreman and by Wujec and Weniger for the lines of multiplet 31 of Cr II are both quite accurate (both have dispersion around our values of substantially less than 0.1 dex), but that the strength of the multiplet as a whole is $\sim$0.5 dex greater than calculated by Kurucz and Peytreman, and $\sim$0.65 dex less than the values inferred by Wujec and Weniger from their adopted calibration. The *gf*-values for lines of multiplet 31 adopted in Table 2 are the Kurucz-Peytreman values, increased by +0.50 dex. Assuming that the relative *gf*-values of Wujec and Weniger are more accurate for comparisons between multiplets, the *gf*-value of the λ4306 line is obtained by correcting the Wujec and Weniger value by −0.65 dex.

Initially I experimented with abundance distributions axisymmetric about the magnetic axis, composed of a constant abundance term plus a term varying as cos α or sin α, where α is the magnetic colatitude. This type of model can be used to describe enhancements or depletions at one or both poles, or around the equator. Typically there would be three free parameters to adjust. Such models work quite satisfactorily for ele-

TABLE 2

CONTRIBUTING SPECTRAL LINES IN SYNTHESIZED REGIONS

Ion (mult)	Wavelength (Å)	log *gf* KP/K	log *gf* Observed	Reference	log *gf* Adopted	Δ log ε
Ca I						
Ca I[a] (5)	4283.010		−0.22 ± 0.10	1	−0.22	0.0
Ca I[a] (5)	4302.527		0.28 ± 0.10	1	0.28	0.0
Ce II[b]	4302.650		−0.55	2	...	...
Cr I and Cr II						
Cr I (131)	4252.243	−1.40	−1.06 ± 0.10	3	−1.40	...
Cr II[a] (31)	4252.62	−2.39	−1.27 ± 0.25	3	−1.89	0.0
Cr I[a] (1)	4254.346	−0.04	−0.11 ± 0.05	1, 4	−0.11	−0.1
Pr II[b] (27)	4254.41	...	−0.69	2	...	...
Cr II[a]	4254.55	−1.16	...		−1.16	−0.2
Cr I (96)	4261.354	−0.49	−0.75 ± 0.10	3	−0.49	...
Pr II[b] (23)	4261.796	...	−1.47	2	...	...
Cr II (17)	4261.80	−3.52	...		−3.52	...
Cr II[a] (31)	4261.92	−1.93	−0.79 ± 0.10	3	−1.43	...
Gd II[b] (44)	4262.092	...	...		...	...
Cr I (154)	4262.38	−1.03	...		−1.03	...
Cr I[a] (1)	4274.803	−0.16	−0.23 ± 0.05	1, 4	−0.23	+0.5
Ce II[b] (206)	4275.561	...	−0.89	2	...	...
Cr II[a] (31)	4275.57	−2.12	−0.88 ± 0.25	3	−1.62	...
La II[b] (40)	4275.64	...	−1.75	2	...	...
Cr II[a] (31)	4284.21	−2.25	−1.11 ± 0.25	3	−1.75	−0.1
Nd II[b] (10)	4284.518	...	−0.73	2	...	...
Cr II (96)	4284.725	−1.22	...		−1.22	...
Fe I (691)	4306.58	−1.91	...		−1.91	...
Ce II[b] (1)	4306.724	...	−0.38	2	...	...
Cr II[a]	4306.93	−1.41	−0.57 ± 0.10	3	−1.22	+0.4
Fe I and Fe II						
Cr I (154)	4271.061	−0.75	−0.83 ± 0.12	3	−0.75	...
Fe I[a] (152)	4271.159	−0.44	−0.35 ± 0.01	5, 6	−0.35	+0.2
Fe I[a] (42)	4271.764	0.19	−0.16 ± 0.01	7	−0.16	0.0
Ti II (95)	4271.931	−3.47	...		−3.47	...
Pr II[b] (15)	4272.271	...	−0.75	2	...	...
Cr I (96)	4272.910	−0.78	−0.99 ± 0.10	3	−0.99	...
Fe II[a] (27)	4273.317	−3.33	−3.28	8	−3.28	0.0
Ce II[b]	4273.440	...	−0.58	2	...	...
Fe I (478)	4273.870	−1.27	...		−1.27	...
Fe I[a] (71)	4282.406	−0.69	−0.75 ± 0.10	1	−0.75	0.0
Pr II[b] (19)	4282.440	...	−0.58	2	...	...
Gd II[b] (117)	4296.30	...	−0.24	2	...	...
Fe II[a] (28)	4296.567	−3.33	−2.95	8	−2.95	...
Ce II[b] (2)	4296.680	...	0.03	2	...	...
Cr I	4302.762	−0.23	...		−0.23	...
Fe II[a] (27)	4303.166	−2.51	−2.49	8	−2.49	−0.3
Cr II	4303.566	−2.52	...		−2.52	...
Sc II (15)	4314.084	−0.10	−0.10 ± 0.25	1	−0.10	...
Fe II[a] (32)	4314.289	−3.60	...		−3.60	0.0
Nd II[b] (9)	4314.511	...	−1.54	2	...	...
Mn II						
Mn II[a] (7)	4253.02	−1.29	...		−1.29	...
Mn II	4253.170	−2.19	...		−2.19	...
Mn II[a] (6)	4283.772	−2.87	...		−2.87	...
Cr II[a] (31)	4284.21	−2.25	−1.11 ± 0.25	3	−2.25	...
Mn II (6)	4284.425	−2.51	...		−2.51	...
Sr II						
Ce II[b]	4305.140	...	−0.30	2	...	...
Sr II[a] (3)	4305.447	−0.14	−0.11 ± 0.25	1	...	...
Fe I (476)	4305.455	−1.74	−1.22 ± 0.10	6	−1.22	...
Pr II[b] (8)	4305.763	...	−0.81	2	...	...

TABLE 2—*Continued*

Ion (mult)	Wavelength (Å)	log *gf* KP/K	log *gf* Observed	log *gf* Reference	log *gf* Adopted	Δ log ϵ
		Ti I and Ti II				
Ti II[a] (20)	4287.893	−1.90	−2.01 ± 0.25	9	−2.01	0.0
Fe I	4287.936	−2.12	...		−2.12	...
Fe I (273)	4288.148	−1.77	−1.86 ± 0.10	6	−1.86	...
Fe I (416)	4299.65	−1.91	...		−1.91	...
Cr I (96)	4299.718	−0.89	...		−0.89	...
Ti II[a] (41)	4300.052	−0.47	−0.75 ± 0.10	9	−0.75	(0.0)
Cr I	4300.126	−0.53	...		−0.53	...
Fe I (975)	4300.196	−2.19	...		−2.19	...
Ce II[b] (134)	4300.331	...	−0.45	2	...	...
La II[b] (9)	4300.44	...	−2.36	2	...	...
Cr I	4300.498	−0.58	...		−0.58	...
Ti II	4301.457	−1.69	...		−1.6	0.0
Ti II[a] (41)	4301.928	−1.28	−1.43 ± 0.10	9	−1.43	...
Pr II[b] (32)	4302.100	...	−1.61	2	...	...
Fe I (520)	4302.191	−1.75	−1.68 ± 0.10	6	−1.68	...
Cr I (177)	4312.469	−1.24	...		−1.24	...
Ti II[a] (41)	4312.861	−1.15	−1.31 ± 0.10	9	−1.31	(0.0)
Fe II (220)	4313.034	−2.06	...		−2.06	...
Ce II[a]	4313.100	...	−1.61	2	...	...

[a] Principal line of a blend.

[b] Rare earth line, not included in calculation.

REFERENCES.—(1) Wiese and Martin 1985; (2) Corliss and Bozman 1962; (3) Wujec and Weniger 1981; (4) Blackwell, Menon, and Petford 1984; (5) Blackwell *et al.* 1982; (6) Fuhr *et al.* 1981; (7) Blackwell *et al.* 1980; (8) Moity 1983; (9) Wise and Fuhr 1975.

ments that have only mild abundance variations, but are entirely unable to introduce enough abundance contrast between high and low abundance regions to describe a very nonuniformly distributed element such as Ti. It was found that with this type of model, if the abundance is high enough to reproduce the strength of the observed Ti lines near $\phi = 0.80$, then no choice of parameters allowed the line to be as weak as demanded by observation at $\phi = 0.30$.

For this reason, the smoothly varying models were discarded in favor of rings or caps of constant abundance. In order to keep the number of free parameters to a minimum, the colatitude α of boundaries between rings of differing abundance is not varied except by varying the total number of zones. Instead, the star is divided into a small number of zones by lines of constant colatitude which are uniformly spaced in α. Within each zone the abundance is given a constant value. The number of zones used is the smallest number that gives a reasonable fit to the observed line profiles. In fact, for 53 Cam all the elements studied can be modeled adequately with three zones, so that normally the abundance distribution is specified by only three parameters.

After some experimentation, it was found that a model distribution could be made to converge satisfactorily toward a reasonable model of a single line if the line profiles are computed for rotation phases more or less centered over each of the zones, and the assumed abundance of each zone is adjusted in the direction indicated by the sense of the discrepancy between the calculated and observed line at the observational phase corresponding to each zone. The line profile at each phase is, of course, affected by other zones than the one crossing the center of the visible disk, but the effect of the central zone on the corresponding line profile is perhaps twice as large as the effect of a zone on the limb, and in practice convergence is quite rapid, with only a few iterations required. The number of zones is set by increasing the number from one (uniform distribution) until a satisfactory solution is obtained. Because the line of sight to 53 Cam passes near both poles and over the equator, the abundance in the cap between $\alpha = 0$ and 60° (around the strong pole) was adjusted using the spectrum observed at $\phi = 0.80$, the equatorial ring was adjusted using the spectrum from $\phi = 0.05$, and the weak pole cap was set using the spectrum at $\phi = 0.30$.

In establishing the abundance distribution, the same distribution was enforced on all lines modeled, but to allow for possible errors in the oscillator strengths, the scale of the abundance was varied from line to line. For Cr, the model was established essentially by comparisons between observations and calculations for the two unblended Cr II lines $\lambda\lambda$4252 and 4284, and then was tested on other lines. The best fit to the observations is found to result from the distribution given in Table 3. The abundance scale found for $\lambda\lambda$4252 and 4284 is essentially the same, differing by only 0.1 dex. This distribution deviates only slightly from a uniform distribution, with abundances in the two polar caps about a factor of 2–3 larger than in the equatorial ring. I cannot securely exclude the possibility that the distribution is exactly uniform, although a uniform model gives a significantly worse fit to the observations than the adopted model. A distribution with a greater abundance contrast between equator and poles than that of the model of Table 3 was also tried; for abundances differing from those of Table 3 by a factor of 2 or so, the fit is also significantly worse.

Tests of the adopted model on other Cr I and Cr II lines

TABLE 3

BEST-FIT MODEL ABUNDANCE DISTRIBUTIONS

ELEMENT	$\log \epsilon_\odot$	$\log \epsilon$ (53 Cam) 0°–60°	60°–120°	120°–180°
Ca	−5.7	$\lesssim -6.1$	$\lesssim -6.1$	−4.3
Cr	−6.4	−4.9	−5.2	−4.2
Fe	−4.5	−3.6	−3.9	−3.4
Mn	−6.5	$\lesssim -5.7$	$\lesssim 5.7$	$\lesssim -5.7$
Sc	−9.0	−9.3:	−9.3:	−9.3:
Sr	−9.1	−5.7	−6.4	−6.2
Ti	−7.1	−5.8	−6.9:	−7.9:

confirm that it is roughly correct, but since most of the other Cr lines are significantly blended (often with rare earth lines not included in the computations), the models for most of these lines do not fit as well as those for λλ4252 and 4284. The best calculated models are shown in Figure 1 for four phases. For each line with which an independent abundance scale value can reasonably be determined, the deviation $\Delta \log \epsilon = \log (\epsilon_{\rm line}/\epsilon_{\rm model})$ is tabulated in the final column of Table 2. It may be seen that the concordance is reasonably satisfactory, both among the Cr II lines and in comparison with the Cr I lines. Only the λλ4274 and 4306 lines show substantial discrepancies from the other lines, and even including these lines (one a resonance line from a very slightly populated ionization stage, the other a high-excitation line with a poorly determined *gf*-value), the dispersion of abundances from individual lines about the mean is only ∼0.26.

With the adopted oscillator strengths, Cr is overabundant with respect to the Sun by a factor of ∼15 around the equator, and ∼40 at the magnetic poles. (The solar abundances of the elements studied are listed in Table 3 along with abundances derived for 53 Cam.)

c) *Abundance Distribution of* Fe

Examination of the spectra of 53 Cam, and comparison with spectra of other Ap and normal stars suggested that the most suitable lines of Fe I for modeling would be the lines at λλ4271.2 ($z = 1.50$), 4271.7 (1.10), and 4282 (1.33), while the best Fe II lines appeared to be λλ4273 (2.17), 4303 (1.47), and 4314 (0.50). The Fe II lines λλ4258.1 and 4258.3 were avoided because they are comparable in strength and blended by the field with each other; the line λ4296 seems to be blended with several moderately strong rare earth lines and was examined only briefly. The Fe II line λ4314, which was modeled, is blended with a line of Sc II, but not strongly enough to warrant dropping the line; in fact, a rough Sc abundance has been derived using this blend.

All the strong Fe I lines modeled have reliable experimental oscillator strengths, but the only NBS evaluated experimental value available for the Fe II lines is for λ4303 (Fuhr *et al.* 1981). For the other lines, we have Kurucz's (1981) theoretical *gf*-values and recent experimental oscillator strengths obtained by Moity (1983). There are substantial differences among these three sources, but preliminary astrophysical *gf*-values obtained by Sigut and Landstreet (1988) are in excellent agreement with values found by Moity, whose results have been adopted in Table 2.

Preliminary modeling indicated that the global abundance of Fe is not far from $\epsilon_{\rm Fe} \sim 2 \times 10^{-4}$, and that, like Cr, the Fe is more or less uniformly distributed. The two Fe I lines at 4271 Å and the Fe II λ4273 line seem to be relatively unblended, and the abundance distribution model was refined by comparison with observations of these lines at various phases in the same way as for Cr. The adopted abundance model was then used to compute the other modeled lines, adjusting only the overall abundance scale to improve agreement.

The adopted abundance distribution is given in Table 3, and corresponding computed line models are shown in Figure 2. The distribution is rather similar to that for Cr, with an overabundance around the magnetic equator of about a factor 4, and polar cap overabundances of 10. Again I cannot completely exclude the possibility that Fe is uniformly distributed, but the adopted distribution gives somewhat better fits to the observations than a uniform distribution. Examination of the model line profiles in Figure 2 reveals that they reproduce the observed profile variations fairly well, including even the complex magnetic structure seen in λ4273.

The change to the overall scale of the abundance distribution required to get the best fit to individual lines is again tabulated in the last column of Table 2 for each line for which it could be determined. It is seen that the abundance scales required to fit the various lines modeled are quite satisfactorily concordant, with deviations from the adopted model of at most ∼0.3 dex.

d) *Abundance Distribution of* Ti

The λλ4250–4315 spectral region contains a number of Ti I and Ti II lines. None of the Ti I lines is strong enough to identify, but several Ti II lines are quite prominent around $\phi = 0.80$. However, all of these same lines are quite weak in the phase range between 0.15 and 0.45, when the weak positive magnetic pole is in view. It is immediately obvious that the variation of the Ti abundance over the stellar surface is far more extreme than that of Cr or Fe.

Several lines of multiplet 41 are strong, as in λ4287 of multiplet 20. Of these lines, λ4290 is blended with the very strong λ4289 line of Cr I, while λλ4307 and 4314 are blended with strong Fe I lines. None of these lines is useful. However, λ4287 ($z = 1.50$) of multiplet 20 and λλ4300 (1.21), 4301 (0.83), and 4312 (1.49) of multiplet 41 are all sufficiently free of strong blending to be worth studying.

In contrast to Cr II and Fe II, the Ti II lines studied all have accurate experimental oscillator strengths which are also in good agreement with the Kurucz-Peytreman values. These are listed in Table 2. Because the experimental oscillator strengths are reasonably accurate, I have adopted these for the analysis. Furthermore, in view of the accuracy of the *gf*-values, I do not let each line determine the abundance separately, but find a best fit for all four lines simultaneously.

A preliminary reconnaissance using a constant abundance in each hemisphere suggests that the abundance is about $\epsilon_{\rm Ti} \sim 2 \times 10^{-6}$ near the strong magnetic pole but $\sim 3 \times 10^{-8}$ around the weak pole. In addition, it appears that all four good Ti II lines have important blends, at least over the part of the star visible when the Ti lines are weak, as is indicated by the varied shapes and diverse radial velocities of the spectral features seen at the positions of these four lines when they are weakest. The impression of significant blending is confirmed by detailed modeling; the shapes and approximate strengths of the four lines can be well reproduced near $\phi = 0.80$, but the profiles of these same lines when they are weak enough to fit within the observed profiles at $\phi = 0.30$ fill only parts of the observed features.

Because the Ti lines are so weak for almost half the rotation period of the star, they provide rather weaker constraints on the form of the appropriate model than is the case for Cr or Fe. The most straightforward interpretation of the observations suggests that they should be modeled with either a two- or three-zone distribution with a large abundance around the negative pole and low abundance at the positive pole (and around the equator for a three-ring model). However, it is also possible to imagine a three-zone model with similar abundances at both poles and a lower abundance around the equator, with the weak line strength near $\phi = 0.30$ due to a substantially smaller size of the positive pole cap compared to the negative pole cap. These various possibilities were all explored.

A two-zone model has the abundances in the two hemispheres fixed at $\sim 9 \times 10^{-7}$ and 2×10^{-8} by comparison with the observed line at $\phi = 0.80$ and 0.30, respectively. At $\phi = 0.80$, quite good fits can be obtained for $\lambda\lambda$4287 and 4301. The calculated profile of λ4300 lacks the observed wing on the long-wavelength side. The wings of λ4312 are fitted quite well, but the observed core is deeper than calculated; either an unidentified blend has essentially the same wavelength as the Ti line, or the *gf*-value (or our model) of this line is in error. At $\phi = 0.30$, none of the calculated lines closely resemble the observed features; the value of the abundance in this hemisphere is determined by increasing it until the calculated profile of the λ4300 line (which has the largest oscillator strength of those considered) touches the observed line. The model is then tested by comparing predicted profiles at $\phi = 0.05$, with observations. The computed $\lambda\lambda$4287 and 4301 lines are clearly much stronger than those observed, and this model may be ruled out as inappropriate. *The extent of the high abundance region around the negative pole is smaller than one full hemisphere.*

A three-zone model with boundaries at $\alpha = 60°$ and 120° as usual was also tried. The abundance around the strong pole is fixed by fitting primarily the $\lambda\lambda$4287 and 4301 lines at $\phi = 0.80$, yielding an average abundance in this cap of $\sim 2 \times 10^{-6}$, more than 20 times the solar value. The abundances in the equatorial ring and the cap around the weak pole were then set by raising their values until the calculated $\lambda\lambda$4287, 4300, and 4301 lines are as deep as allowed by the observations. The resulting abundances are $\sim 1.3 \times 10^{-7}$ around the equator and 1.3×10^{-8} around the positive pole. The model line profiles, shown in Figure 3, do not fit the observed ones very accurately but do account for the general strength of the observed features; remaining parts of the profile are mostly plausibly due to uncalculated rare earth blends. This model may be given one further test by computing the profiles of the nearly unblended λ4468 and only mildy blended λ4501 lines observed in one spectrum taken at $\phi = 0.166$ (see Table 1). Both lines are reasonably well accounted for by this model; in restrospect, these would probably have been better lines to observe to model Ti in 53 Cam.

To try to test the uniqueness of the three-zone model derived above, several other types of models were explored. (1) I tried having the whole region around 60° and 180° have a single uniform abundance. When this model fits at $\phi = 0.80$ and $\phi = 0.30$, it predicts line profiles near $\phi = 0.05$ that are much too weak. (2) Another possibility, suggested by MMC, is to have a very low equatorial abundance (say 10^{-4} of the value around the negative pole). Again, such a model predicts line profiles at $\phi = 0.05$ that are much shallower than observed and also leads to a much weaker λ4501 line than is observed at $\phi = 0.17$. (3) Finally, again trying to employ the type of model suggested by MMC, I considered having the same abundance at both polar caps, but a smaller polar cap around the positive pole than around the negative one. In such a model, the cap around the positive pole can extend to no more than $\sim 30°$ from the pole, and if it extends this far, the observed $\lambda\lambda$4300 and 4301 lines at $\phi = 0.05$ and the $\lambda\lambda$4468 and 4501 lines at $\phi = 0.17$ are much stronger than predicted. In order for a high abundance patch to occur at the positive pole, it must be confined to such a small region (say within $\sim 15°$ of the pole) that it makes very little contribution to the integrated profiles at any phase, and we are back to the three-zone model originally derived, with a minor, almost invisible, change.

Thus, modeling leads to the fairly unambiguous result that the abundance of Ti around the negative pole is ~ 20 times solar, while the abundances around the equator and the positive pole are, respectively, ~ 10 and 100 times lower. It seems impossible to escape the conclusion that *Ti is distributed in an exceedingly nonuniform fashion on 53 Cam*, and that *a very large difference in abundance* (averaged over a large area) *exists between the two poles.*

e) *Abundances of Other Elements*

No lines of chemical elements other than Cr, Fe, and Ti are present in the $\lambda\lambda$4250–4315 region with sufficient purity and strength to make possible the derivation of good abundance maps. Nevertheless, enough lines of several other elements are present (or absent) that it is possible to derive some useful limits on the abundances of Ca, Sc, Mn, and a few rare earths.

Ca is present in my spectra in the form of a strong and quite variable K line in the $\lambda\lambda$3900–3960 spectra. The line always has a strong core, but has greatly enhanced damping wings in the spectra at $\phi = 0.17$ and 0.29, near positive field extremum. However, I cannot yet model this line with the line synthesis program because of a lack of a version of the program that can work economically on a large-wavelength window, and because I have not yet studied the region closely enough to identify and assess the importance of the numerous blending lines that litter the wings of the K line. For the present, quantitative analysis must be based on two lines of Ca I of multiplet 5, $\lambda\lambda$4283 and 4302, which are clearly visible in spectra at $\phi = 0.18$, 0.30, and 0.42, but are otherwise not detected (see Fig. 2). These lines can be approximately modeled with a large Ca-rich spot around the positive magnetic pole, and a uniform lower abundance elsewhere. If the enhanced spot is taken to extend from $\alpha = 120°$ to 180°, the inferred abundance is ~ 20 times the solar value. In the larger region of low abundance the absence of the two lines of Ca I allows one only to set an upper limit to the abundance, but the appearance and lack of strong variability of the K line from $\phi = 0.55$–0.04 strongly suggests that the abundance in the depleted region is roughly uniform. On this assumption, the upper limit to the abundance in the low abundance region is found to be ~ 60 times smaller than that in the enhanced region, with an abundance of less than about half the solar value. Details are given in Table 3. Note that although the oscillator strengths of the two Ca I lines used are quite accurate, the scale of the abundance of Ca is uncertain because it is based only on lines of the neutral atoms rather than the dominant first ion. Still, the large ratio between the abundance averaged over the enhanced cap and that found over the remainder of the star should not be too sensitive to scale problems, and the conclusion that the abundance contrast of this element is large seems fairly secure. Thus, we find

Ca to have an abundance distribution reminiscent of that of Ti, with one region in which the local abundance is enhanced with respect to the rest of the star by a factor of order 10^2, but *for Ca the enhanced region is around the weaker positive pole rather than the strong negative one.* (Of course, it is again possible that a sufficiently small region of high abundance may exist at the negative pole.)

Sc II is represented by one line at 4314.084 Å which is blended with the stronger Fe II line at 4314.289 Å. An asymmetry and radial velocity shift of this feature relative to other Fe II lines makes it clear that the Sc blend is present. It is difficult to obtain a reliable abundance for this line even at $\phi = 0.30$, when the lines are sharpest, but it appears that ϵ_{Sc} is very roughly 6×10^{-10} uniformly over the star. The models of the λ4314 blend in Figure 2 have been calculated with this abundance. It is noteworthy that the derived Sc abundance is only about a factor 2 below the solar abundance.

Several lines of Mn would be present in the $\lambda\lambda$4250–4315 region if the Mn abundance were high. Of these, the lines most nearly in clear regions are $\lambda\lambda$4253 and 4283 of multiplets 7 and 6, respectively, of Mn II. These lines are quite strong in spectra of Mn-rich stars such as ν Her, ι CrB, and HD 111133. The λ4253 line has the larger *gf*-value and allows us to set the most stringent abundance limit. From the observed absence of this line at all phases (see Fig. 1), the abundance of Mn appears to have an upper bound of $\sim 2 \times 10^{-6}$ (a value ~ 6 times the solar abundance) over the entire stellar surface.

Sr has one strong line of the first ion at 4305 Å. The observed line has strong blends in both wings, probably due to lines of Ce II and Pr II each ~ 0.3 Å from the Sr line, and virtually coincides with a line of Fe I. The coincidence of the Sr line with the blending Fe line raises the question of which of the two lines produces the observed feature. Fortunately, the Fe line has a well-determined *gf*-value, and calculation using the adopted Fe model and the Fe line alone produces a feature much weaker than the observed one. It thus seems clear that Sr is present. A model was derived in the same way as the others, fitting to the core of the observed feature but ignoring the wings. The best model, tabulated in Table 3, is intermediate between those found for Cr and Fe and those of Ti and Ca: there seems to be a significant enhancement at the negative pole relative to the rest of the star, but only by a factor of ~ 4. The absolute abundance for Sr is found to be very much larger than in the Sun; the abundance at the negative pole is ~ 2000 times larger than the solar value, and over the rest of the star the abundance is more than 500 times larger than solar.

It seems clear that many of the rare earths are somewhat overabundant in 53 Cam, although they are not as prominent in 53 Cam as in some cool Ap stars such as β CrB and HD 125248 = CS Vir. Both Babcock (1958) and Faraggiana (1973) note strong Eu, which Faraggiana finds to be variable. Cowley (1986), using line coincidence statistics, positively identifies La II and Ce II in a spectrum of 53 Cam apparently taken near Ti maximum. In my own spectra, the Gd II lines at 4251.71, 4253.37, and 4253.61 Å are clearly present. Furthermore, many of the lines studied above are definitely blended with subsidiary lines most readily identified in most cases as due to rare earths. However, in my spectra almost no isolated rare earth lines occur. This makes it quite difficult to do more than set rough limits on abundances of a few elements. In no case are the data good enough to establish abundance maps without a large amount of additional effort and uncertainty, and it is for this reason that I have chosen not to include rare earth blends in syntheses of iron peak elements: including the rare earth lines in most cases simply introduces too many free parameters.

However, I have done some preliminary experiments in modeling a broad feature on the short-wavelength wing of the λ4296 line of Fe II, which seems to be produced by a blend of La, Ce, and Gd lines. If all these elements are assumed to have uniform abundances of $\sim 1 \times 10^{-8}$ the observed feature may be approximately reproduced. This suggests that the rare earths are present with abundances of the order of 400 times solar.

f) Uncertainties of the Model

A number of sources of uncertainty and error have alrready been discussed above. These include imprecise *gf*-values; blends, mainly by overabundant rare earths, which afflict most lines of all elements modeled to at least some extent; some residual uncertainty as to how accurate the magnetic model is, especially near the equator where small systematic differences between observed and calculated lines persist even for the best-fit lines such as $\lambda\lambda$4252 and 4284 of Cr II; and the crudeness of the adopted abundance distribution geometry. Of these problems, the oscillator strength uncertainties for the ions probably loom largest in determining the errors of the scale of the abundances chosen, while the coarseness of the abundance distributions probably dominates uncertainties in relative abundance distributions, at least for those elements like Cr and Fe that show clear lines at all phases. Uncertainty in mapping more nonuniformly distributed elements such as Ca and Ti is probably dominated by the effects of blends in distorting or concealing lines for part of the stellar rotation period.

A further source of uncertainty is the choice of an appropriate model atmosphere. I have used throughout a Muthsam (1978) model atmosphere of $T_e = 8500$ K and $\log g = 4.0$, whose *UBV* colors are quite close to those observed for 53 Cam. This model was constructed assuming abnormally high abundances of most metals compared to the solar abundances, which leads to somewhat steeper temperature stratification $T(\tau_0)$ than is found in a normal atmosphere of the same T_e and g. To test the uncertainties introduced into the analysis that stem from uncertainty in the appropriate model atmosphere, I have recalculated a few theoretical lines using two different Kurucz (1979) atmosphere models whose *UBV* colors are also quite close to those observed for 53 Cam. These atmospheres have $T_e = 8000$ K and $\log g = 3.5$, and $T_e = 8500$ K and $\log g = 4.0$. These two model atmospheres are different enough from the adopted one that the changes that result from using one or the other in place of the Muthsam atmosphere should give an adequate estimate of uncertainties stemming from the choice of atmosphere.

When lines of first ions are recalculated using the Kurucz 8500 K model, they are virtually unchanged. Use of the 8000 K atmosphere strengthens the ion lines somewhat, but not enough to reduce an overall abundance scale determined from ion lines by more than a factor of 2. Neutral lines, of course, are more sensitive; even changing from the 8500 K Muthsam atmosphere to the 8500 K Kurucz atmosphere can reduce the derived abundance scale by a factor of more than 2, and the change is about as large in going to the 8000 K Kurucz atmosphere. Thus the abundance scale determinations, to the extent that they are based on (dominant) first ions, are not made substantially less accurate by uncertainty as to the best model atmosphere, while abundances based on neutral lines (Ca I) have choice of the model atmosphere as the dominant

uncertainty in the abundance scale. Of course, choice of the atmosphere model should have only a very small effect on the abundance distribution found.

V. DISCUSSION

a) Comparison with Previous Models

It is of interest to compare the results of this modeling to previous work. My magnetic model is qualitatively quite similar to those of Huchra (1972), Borra and Landstreet (1977), MMC, and Landi Degl'Innocenti *et al.* (1981), except for the addition of a modest octupole component that does not change the global morphology of the field. Both the field strength parameters B_d and B_q and the angles i and β have changed little, by a few percent and a few degrees, respectively. The overall field structure model is simply refined by these calculations.

Comparison with the one previous abundance distribution model of this star, due to MCC is more interesting. They give their model a physical basis as a plausible result of diffusion in the presence of a strong magnetic field. The basic structure of their model results from the prediction that iron peak elements will tend to accumulate where the magnetic field is vertical, that is, in caps near the poles, while rare earths will tend to accumulate where field lines are horizontal, in a band around the magnetic equator. Starting from this basic premise, they fit Faraggiana's spectrum variation observations, and Borra and Landstreet's and Huchra's magnetic measurements, using a dipole plus quadrupole field configuration, and an abundance model with constant ϵ in a ring or two caps of adjustable size and $\epsilon = 0$ elsewhere. Their computed local spectral line intensity profiles are broadened only by thermal Dopper motions, and the theory used for the local line profiles is very simple and includes no magnetic effects.

MMC find that with a small Fe-rich cap around the positive magnetic pole and a considerably larger one around the negative pole, they are able to satisfactorily reproduce Faraggiana's observations of the variation of the equivalent width typical iron lines. They also find that with an equatorial ring of Eu they can fit the observed variation of that element. However, when they predict the effective fields that should be observed using the Fe or Eu lines, the predicted curves deviate greatly both from the measurements made using the Hβ line and from photographic measurements based on metal lines. Similarly, the predicted surface field curves are different from the observed values. They speculate that substantial differences may have been present between observed field strengths measured with spectral lines of various elements that were not mentioned by Babcock or Huchra.

The basic distribution model adopted here is deliberately very similar in structure to that used by MMC, except that the boundaries of my rings and caps are variable only by varying the number of zones, while each of my zones has a separately determined abundance. For both Fe and Cr, I do in fact find a two-cap structure to the abundance distribution, with higher abundances (by a factor of 2 or 3) near the poles than around the equator. In contrast, Ti and Ca each appear to be concentrated in a single cap, Ti around the negative pole and Ca arund the positive pole, with abundance lower by a factor of 10–100 outside the cap. The results of my modeling suggest that MMC's assumption of $\epsilon = 0$ between the caps is quite a poor approximation, especially for Fe and Cr. In fact, for both these elements the model lines fit the present observations only a little worse, assuming completely uniform abundance distributions than with enhanced polar caps. It must be emphasized that almost all the equivalent width variations observed by Faraggiana are due to variations in the broadening produced by the global magnetic field as seen from various directions. The very high abundance contrasts assumed by MMC are only found for Ti and Ca, and these elements still possess detectable lines even when the high abundance caps are fully out of sight.

The difficulty that MMC had in accounting for the magnetic field observations is relieved when my distribution model is substituted for theirs. Although neither Babcok or Huchra is very explicit about what lines were used to measure the magnetic field, their measurements must have been based primarily on lines of Fe and Cr, since the Ti lines are extremely variable and the rare earth lines are mostly too weak to use. Thus both the photographically measured B_e and B_s curves must have been based almost entirely on two elements that are nearly uniformly distributed, and which therefore actually measure something close to the calculated B_e and B_s values. The problem that MMC have in accounting for the observed magnetic field curves comes almost entirely from their modeling assumption that ϵ, and therefore the contribution to each integrated line profile, vanish over large parts of the stellar disk.

MMC also predict that line profiles of the iron peak elements should show very strong changes in shape and radial velocity due to the abundance variations. In fact, almost all the profile variations of Cr and Fe lines, which are typically of the order of 20% peak to peak, are due to magnetic intensification. The profiles of the Ti and Ca lines observed do undergo drastic changes, but unfortunately for much of the rotation period the behavior of these lines is confused by blends.

The result of my modeling of 53 Cam is that both Ti and Ca show evidence of concentration at only one of the two magnetic poles. It is not obvious on the basis of the MMC model of horizontal diffusion why this should occur, or why Ti and Ca should concentrate at opposite poles. Instead, this result suggests to me that another mechanism may be influencing diffusion in addition to any horizontal drift high in the atmosphere, namely the effect of the field in desaturating the spectral lines by which radiation pressure is transmitted to ions. This effect (which was briefly discussed by MMC) is certainly different at the two poles, and may provide a more natural explanation of the observed concentrations of Ti and Ca.

b) Size and Mass of 53 Cam

Another interesting result of modeling the magnetic field is that it leads to a reasonably precise value of the stellar radius, and thus also of the luminosity and evolutionary state of 53 Cam. The estimate of the radius is made using the elementary relationship

$$R/R_\odot = Pv \sin i/(50.6 \sin i)\,, \qquad (11)$$

where P is in days and $v \sin i$ in km s^{-1}. Taking $v \sin i = 13 \pm 1.5$ km s^{-1} as determined from Cr line fitting, and $P = 8.03$ days with negligible uncertainty, we can estimate R if sin i is known. We have considered a variety of magnetic field models, but all fits require $i \geq 60$. Even if we take $i \geq 50°$ to include the model adopted by Michaud, Megessier, and Charland (1981), we still have sin $i = 0.89 \pm 0.11$. Combining these values, we find log $(R/R_\odot) = 0.365 \pm 0.07$, or $R/R_\odot = 2.32 \pm 0.40$. This value has quite respectable accuracy even when compared to direct determinations (see Shallis *et al.* 1985). Now it seems unlikely that the adopted effective tem-

perature is in error by more than ~500 K (Faraggiana 1973 estimates that it lies in the range 8160–8810 K from a variety of photometric methods; see also Stępień 1980). Taking $T_e = 8500 \pm 500$ K leads to $\log (L/L_\odot) = +1.40 \pm 0.17$, or $L/L_\odot = 25 \pm 10$. Plotting these values in the Hertsprung-Russel (H-R) diagram with the main-sequence models of Alcock and Paczyński (1978) leads to an estimate of $M/M_\odot = 2.0 \pm 0.3$, so that $\log g = 4.0 \pm 0.25$, consistent with the gravity of the adopted atmosphere model. The location of 53 Cam in the H-R diagram on the evolutionary track of a 2 $M_\odot$ star is fairly sensitive to the metal abundance Z assumed in construction of the main-sequence model; for $Z = 0.03$, 53 Cam lies roughly in the middle of the main-sequence track, while for $Z = 0.01$, the star seems to be near the end of main-sequence core H burning. In any case, it seems unlikely that 53 Cam is a really young star. This fact is of significance for attempts to understand how the star came to have its present surface abundance distribution, especially as it is quite likely that surface abundances evolve with time.

c) *An Alternative Method for Measuring B_s*

One final interesting result of the present study is that it suggests that it may be possible to use magnetic intensification of spectral lines as a means of measuring the surface field strengths of some magnetic Ap stars in which $v \sin i$ is somewhat too large to measure B_s by using line widths. For example, in the spectral region studied, Cr II λ4252 has a somewhat smaller value of gf than λ4284, but for fields of 10 kG or more, the equivalent width of λ4252 is ~50% greater than that of λ4284. This effect could only be used for stars of unusually large surface fields, and the problem of possible blends would have to be considered, perhaps by using a number of suitable line pairs, but this technique offers the possibility of adding several more stars to the very short list for which B_s has been measured and a well-defined magnetic model derived.

VI. CONCLUSIONS

We may summarize the results of this study as follows. An extensive data set has been obtained for the magnetic Ap star 53 Cam, consisting of Balmer line Zeeman analyzer measurements of the longitudinal magnetic field and high signal-to-noise spectra with a resolution of 0.1 Å of the regions $\lambda\lambda$3900–3960 and 4250–4315. The data are well spaced through the 8.03 day rotation period of the star. These data have been used to define the magnetic field geometry and the abundance distributions principally of Cr, Fe, and Ti through the use of a line synthesis program. This program starts with a specified model magnetic geometry and assumed abundance distributions for one or several chemical elements. Both the magnetic geometry and the abundance distributions are specified with a small number of parameters. The magnetic field is allowed to have colinear dipole, quadrupole, and octupole components aligned at an oblique angle β to the stellar rotation axis. The abundance distributions used are (usually three) zones of constant abundance, axisymmetric about the magnetic field axis and of equal width in colatitude. Using the available data and these models, it has been found practical to iterate both field and abundance geometries to distributions that predict reasonably well the strengths, profiles, and variations of a number of spectral lines. Although the resulting models are incapable of describing small-scale structure (if there is any) on 53 Cam, they appear to be reasonably unique and may well be low resolution but essentially correct representations of the star, provided that small-scale structure or effects omitted altogether (such as possible depth dependence to local abundances) are not important.

The polar field strengths of the field components in the final magnetic model are $B_d = -16{,}300$ G, $B_q = -7300$ G, and $B_0 = 4900$ G. The dipole and quadrupole components found are similar to those found in previous modeling efforts. The octupole component is required by the widths of spectral lines observed at phases when the longitudinal magnetic field is passing through zero. The obliquity β and inclination i of the rotation axis to the line of sight are both large (~64° and 82°, but it is not clear from the present data which angle has which value).

The elements Cr and Fe have similar abundance distributions, with abundances somewhat lower (by a factor of order 2) around the magnetic equator than at the magnetic poles. There is some indication that the abundances of these elements may be slightly larger at the weaker positive magnetic pole than at the stronger positive pole. The mild equivalent width variations ($\pm$10%) observed for lines of Cr and Fe are due almost entirely to magnetic effects. The global Fe abundance is ~10 times larger than solar. The global Cr abundance seems to be ~30 times solar, but this is still somewhat uncertain because of the serious discrepancies between theoretical and experimental oscillator strengths.

In contrast, Ti is very nonuniformly distributed. It appears to occur in a patch of ~10 times solar abundance around the strong negative magnetic pole, to have approximately solar abundance around the equator, and to be almost 10 times underabundant at the positive pole. This behavior is apparently mimicked by Ca, but it is overabundant around the weak positive pole. For each of these elements, if there is a region of high abundance at the low abundance pole, it must be much smaller than the similar cap at the opposite pole. Probably the most significant result of this study is to establish that the surface abundance distributions of several iron peak elements on 53 Cam are grossly dissimilar. This clearly offers a significant clue to the processes leading to the observed surface inhomogeneity.

This project has benefited from the help and advice of a large number of people. R. Wehrse was particularly helpful to me both in offering much useful advice on how to treat problems in radiative transfer, and in arranging for me to spend part of a sabbatical year in Heidelberg, where the line synthesis program was written. In addition, I have had informative and stimulating discussions on the topics of this paper with B. Baschek, D. Bohlender, C. Cowley, G. Michaud, and J. O. Stenflo, among others. J. Fuhr provided valuable advice on the selection of oscillator strength values. Reductions of Canada-France-Hawaii Telescope spectra were carried out using a package of programs kindly provided by P. K. Barker. Data reduction was done by M. Jewison, who also helped to obtain the spectra. A number of calculations for this project were carried out by A. Sigut, who was also very helpful in debugging the line synthesis program. R. Kurucz was kind enough to provide a tape copy of the Kurucz-Peytreman line list to my department. A. Brooks and M. Rasche were very helpful in the work of preparing the manuscript. The referee, C. Megassier, offered a number of helpful suggestions on presentation. This work was supported financially by the Natural Sciences and Engineering Research Council of Canada, and by the Deutsche Forschungsgemeinschaft (both directly and through Sonderforschungsbereich 132).

REFERENCES

Alcock, C., and Paczyński, B. 1978, *Ap. J.*, **223**, 244.
Alecian, G., and Vauclair, S. 1981, *Astr. Ap.*, **101**, 16.
Aller, L. H. 1963, *Astrophysics: the Atmospheres of the Sun and Stars* (New York: Ronald).
Aller, M. F., and Everett, C. H. F. 1972, *Ap. J.*, **172**, 447.
Babcock, H. W. 1958, *Ap. J. Suppl.*, **3**, 141.
———. 1960, in *Stars and Stellar Systems*, Vol. **6**, *Stellar Atmospheres*, ed. J. L. Greenstein (Chicago: University of Chicago Press), p. 282.
Baschek, B., and Scholz, M. 1982, in *Landolt-Börnstein, Zahlenwerte und Funktionen aus Naturwissenschaften und Technik*, Neue Ser., Group VI, Vol. **2b**, ed. K. Schaifers and H. H. Voigt (Berlin: Springer), p. 107.
Beckers, J. M. 1969, *A Table of Zeeman Multiplets* (AFCRL-69-0115).
Blackwell, D. E., Menon, S. L. R., and Petford, A. D. 1984, *M.N.R.A.S.*, **207**, 533.
Blackwell, D. E., Petford, A. D., Shallis, M. J., and Simmons, G. T. 1980, *M.N.R.A.S.*, **191**, 445.
———. 1982, *M.N.R.A.S.*, **199**, 43.
Blackwell, D. E., and Shallis, M. J. 1979, *M.N.R.A.S.*, **186**, 673.
Böhm-Vitense, E. 1965, in *Magnetism and the Cosmos*, ed. W. Windmarsh *et al.* (Edinburgh: Oliver & Boyd), p. 179.
Bolton, C. T. 1970, *Ap. J.*, **161**, 1187.
———. 1971, *Astr. Ap.*, **14**, 233.
Borra, E. F. 1974, *Ap. J.*, **188**, 287.
Borra, E. F., and Landstreet, J. D. 1977, *Ap. J.*, **212**, 141.
———. 1978, *Ap. J.*, **222**, 226.
Borra, E. F., Landstreet, J. D., and Mestel, L. 1982, *Ann. Rev. Astr. Ap.*, **20**, 191.
Campbell, B., Walker, G. A. H., Johnson, R., Lester, T., Yang, S., and Auman, J. 1981, *Proc. SPIE*, **290**, 215.
Carbon, D. F., and Gingerich, O. 1969, in *Theory and Observations of Normal Stellar Atmospheres*, ed. O. Gingerich (Cambridge: MIT Press), p. 399.
Condon, E. U., and Shortley, G. H. 1935, *The Theory of Atomic Spectra* (Cambridge: Cambridge University Press).
Corliss, C. H., and Bozman, W. R. 1962, *NBS Monog.*, No. 53.
Cowley, C. 1971, *Observatory*, **91**, 139.
———. 1986, private communication.
Deridder, G., and van Rensbergen, W. 1976, *Astr. Ap. Suppl.*, **23**, 147.
Deridder, G., van Rensbergen, W., and Hensberge, H. 1979, *Astr. Ap.*, **77**, 286.
Deutsch, A. J. 1958*a*, in *Handbuch der Physik*, Vol. **51**, ed. S. Flügge (New York: Springer), p. 689.
———. 1958*b*, in *Electromagnetic Phenomena in Cosmic Physics*, ed. B. Lehnert (Cambridge: Cambridge University Press), p. 209.
Faraggiana, R. 1973, *Astr. Ap.*, **22**, 265.
Fuhr, J. R., Martin, G. A., Wiese, W. L., and Younger, S. M. 1981, *J. Phys. Chem. Ref. Data*, **10**, 305.
Gingerich, O. 1964, in *Proc. 1st Harvard-Smithsonian Conf. on Stellar Atmospheres* (*Smithsonian Ap. Obs. Spec. Rept.*, No. 167, p. 42).
Goncharskii, A. V., Stepanov, V. V., Khokhlova, V. L., and Yagola, A. G. 1977, *Soviet Astr. Letters*, **3**, 147.
———. 1982, *Soviet Astr.*, **26**, 690.
Goncharskii, A. V., Ryabchikova, T. A., Stepanov, V. V., Khokhlova, V. L., and Yagola, A. G. 1983, *Soviet Astr.*, **27**, 49.
Hardorp, J., Shore, S. N., and Wittmann, A. 1976, in *Physics of Ap Stars*, ed. W. W. Weiss, H. Jenkner, and H. J. Wood (Vienna: Universitätssternwarte Wien), p. 419.
Huchra, J. 1972, *Ap. J.*, **174**, 435.
Khokhlova, V. L. 1970, *Soviet Astr.*, **14**, 107.
———. 1985, *Soviet Sci. Rev. E, Ap. Space Phys.*, **4**, 99.
Khokhlova, V. L., Rice, J. B., and Wehlau, W. H. 1986, *Ap. J.*, **307**, 768.
Khokhlova, V. L., and Ryabchikova, T. A. 1975, *Ap. Space Sci.*, **34**, 403.
Kurucz, R. L. 1979, *Ap. J. Suppl.*, **40**, 1.
———. 1981, *Smithsonian Ap. Obs. Spec. Rept.*, No. 390.
Kurucz, R. L., and Peytremann, E. 1975, *Smithsonian Ap. Obs. Spec. Rept.*, No. 362.
Landi Degl'Innocenti, E. 1976, *Astr. Ap. Suppl.*, **25**, 379.
Landi Degl'Innocenti, M., Calamai, G., Landi Degl'Innocenti, E., and Patriarchi, O. 1981, *Ap. J.*, **249**, 228.
Landstreet, J. D. 1970, *Ap. J.*, **159**, 1001.
———. 1980, *A.J.*, **85**, 611.
———. 1982, *Ap. J.*, **258**, 639.
———. 1987, *M.N.R.A.S.*, **225**, 437.
Martin, B., and Wickramasinghe, D. T. 1979, *M.N.R.A.S.*, **189**, 883.
Megessier, C. 1975, *Astr. Ap.*, **39**, 263.
———. 1984, *Astr. Ap.*, **138**, 267.
Megessier, C., Khokhlova, V. L., and Ryabchikova, T. A. 1979, *Astr. Ap.*, **71**, 295.
Michaud, G. 1970, *Ap. J.*, **160**, 641.
Michaud, G., Megessier, C., and Charland, Y. 1981, *Astr. Ap.*, **103**, 244 (MMC).
Mihalas, D. 1973, *Ap. J.*, **184**, 851.
———. 1978, *Stellar Atmospheres* (San Francisco: Freeman).
Moity, J. 1983, *Astr. Ap. Suppl.*, **52**, 37.
Moore, C. E. 1945, *NBS Tech. Note*, No. 36.
———. 1949, *NBS Circ.*, No. 467.
Muthsam, H. 1978, *Astr. Ap. Suppl.*, **35**, 107.
———. 1979, *Astr. Ap.*, **73**, 159.
Panofsky, W. K. H., and Phillips, M. 1955, *Classical Electricity and Magnetism* (Reading: Addison-Wesley).
Piskunov, N. E. 1986, preprint.
Preston, G. W. 1967, in *The Magnetic and Related Stars*, ed. R. C. Cameron (Baltimore: Mono Book), p. 26.
———. 1969*a*, *Ap. J.*, **156**, 967.
———. 1969*b*, *Ap. J.*, **157**, 247.
———. 1970, *Ap. J.*, **160**, 1059.
———. 1971*a*, *Pub. A.S.P.*, **83**, 571.
———. 1971*b*, *Ap. J.*, **164**, 309.
Pyper, D. M. 1969, *Ap. J. Suppl.*, **18**, 347.
Rice, J. B. 1970, *Astr. Ap.*, **9**, 1970.
Schwarzschild, M. 1950, *Ap. J.*, **112**, 222.
Shallis, M. J., Baruch, J. E. F., Booth, A. J., and Selby, M. J. 1985, *M.N.R.A.S.*, **213**, 307.
Sigut, T. A., and Landstreet, J. D. 1988, in preparation.
Stenflo, J. O. 1971, in *Solar Magnetic Fields*, ed. R. Howard (Dordrecht: Reidel), p. 101.
Stępień, K. 1980, *Astr. Ap.*, **92**, 171.
Unno, W. 1956, *Pub. Astr. Soc. Japan*, **8**, 108.
Van Rensbergen, W., Hensberge, H., and Adelman, S. J. 1984, *Astr. Ap.*, **136**, 31.
Vauclair, S., Hardorp, J., and Peterson, D. M. 1979, *Ap. J.*, **227**, 526.
Wehlau, W., Rice, J., Piskunov, N. E., and Khokhlova, V. L. 1982, *Soviet Astr. Letters*, **8**, 15.
Wiese, W. L., and Fuhr, J. R. 1975, *J. Phys. Chem. Ref. Data*, **4**, 263.
Wiese, W. L., and Martin, G. A. 1985, in *CRC Handbook of Chemistry and Physics*, ed. R. C. Weast (Boca Raton: CRC Press), p. E-325.
Wittman, A. 1974, *Solar Phys.*, **35**, 11.
———. 1977, *Astr. Ap.*, **54**, 175.
Wolff, S. C. 1976, in *Multiple Periodic Variable Stars*, ed. W. S. Fitch (Dordrecht: Reidel), p. 43.
———. 1983, *The A-Type Stars: Problems and Perspectives* (NASA SP-463).
Wolff, S. C., and Wolff, R. J. 1970, *Ap. J.*, **160**, 1049.
Wujec, T., and Weniger, S. 1981, *J. Quant. Spectros. Rad. Trans.*, **25**, 167.

J. D. LANDSTREET: Department of Astronomy, University of Western Ontario, London, Ontario, N6A 3K7, Canada